A Computational Approach to Analyze the Dynamics and Effects of Viscoelastic Ground Contact for Walking Mechanisms

A Computational Approach to Analyze the Dynamics and Effects of Viscoelastic Ground Contact for Walking Mechanisms

A Thesis
submitted in partial fulfillment of the requirements for the degree of
Doctor of Philosophy

by

Dondogjamts Batbaatar
(Student Number: 18899016)

Kyutech
Kyushu Institute of Technology

Graduate School of Life Science and Systems Engineering
Kyushu Institute of Technology
Japan
March, 2021

A Computational Approach to Analyze the Dynamics and Effects of Viscoelastic Ground Contact for Walking Mechanisms

by

Dondogjamts Batbaatar

Submitted to the Graduate School of Life Science and Systems Engineering
on March, 2021, in partial fulfillment of the
requirements for the degree of
Doctor of Philosophy

Abstract

Since animal bodies are highly complex to be organized biologically, it is not easy to evaluate the advantage of flexibility in the musculoskeletal system in comparison with mechanical rigid bodies. For the reason, a simplification had been implemented in traditional scheme of the reduced degree of freedom mechanisms with well-designed fixed limb trajectory for real world applications, and the best mechanical structure was explored to minimize its energy consumption known in walking linkage mechanisms. As the possible hypothesis, the advantage of high energy conservation effect can be maximized according to a smooth grounding at the touching moment of the toe on the ground. The smooth trajectory itself can be reproduced by closed-linkage walking models, while the effect of the interaction between the toe and ground is unclear and viscoelastic contact may enhance the effect. For the clarification of the hypothesis, a fine computational framework is needed to be established to provide less computational cost and enough accuracy and stability in the analysis. Traditionally, the rigid-body mechanics and contact force analysis were separately studied and developed. In the present study, multibody dynamics approach based on the analytical mechanics was newly integrated with the viscoelastic contact force model, which is able to implement a hysteresis damping phenomenon simply. By using the linkage mechanisms, the elasticity of the grounding was analyzed through the inverse dynamics based on the proposed computational framework involving the multibody dynamics and contact force model implementation. The proposed method was located in an intermediate position between the discrete contact model for a less frequency attachment of bodies and the continuous model for stable attachment phenomenon. In the sense, the method was appropriate for analyses of walking mechanisms with a consistent frequency of the attachment with the ground, which requires a fine reaction force analysis. In the computer experiment as the comparison of typical and simplified walking linkage mechanisms, the proposed method applied to Chebyshev and Theo-Jansen walking mechanisms and demonstrated the required torque in the

driving input when those mechanisms were walking on the ground. In an energy analysis, which is defined as the required input-torque integration in a cycle of the leg motion, the perfectly elastic ground contact commonly reduced the energy consumption significantly in the comparison of the coefficient of restitution in the damping factor model by Lankarani and Nikravesh. The result proved the hypothesis of the positive effect of the smooth grounding in the range of the proposed computational approach. It may contribute to providing an criterion not only for a real walking robot design but also assistive devise configurations to absorb unnecessary ground reaction force to prevent the damage to the leg mechanism and enhance a smooth walking pattern.

Keyword

Closed-loop linkages, Multibody dynamics (MBD), Contact force model, Energy consumption, Computational framework.

Acknowledgments

There have been many people who have helped me during this great experience and intense learning period. I would like to give my sincerely thanks to them, to only some of whom it is possible to give particular mention here.

First of all, I would like to thank to my PhD supervisor, Associate Professor Hiroaki Wagatsuma for the good advice, support and guidance that has been valuable on both academic and personal growth. He has been very patiently supervising me and always guiding me in the right direction. I have learned a lot from him, without his help this thesis would not have met an end. In addition, I would like to thanks the member of PhD committee Professor Kazuo Ishii, Professor Eiji Hayashi, Associate professor Horiyuki Miyamoto, Associate professor Hiroaki Wagatsuma for their excellent suggestion and detail review during the thesis evaluation. I am grateful to all lab members, in particular, Jisha Maniamma, Ankur Dixit, Kumar Arvind, Dachkinov Pancho, Yoshitaka Kato, Maria Sanchez, Kazuki Kanamaru, and Takuma Kariya for their support and for the great time we have shared these three years.

Finally, I owe my heartfelt thanks to my close people. I am very grateful for my wife Baigalmaa Gantumur, her understanding encouraged me to work hard. Thanks to my mother Dolgorsuren Purevdorj who always ask for the health and state of the research work, and also thanks to my close friends in Kyutech, who have made the effort to understand that PhD does not let me have so much free time. Last but not least, thank you very much, everyone who directly or indirectly supported and helped me.

Dondogjamts Batbaatar

Contents

List of Figures

List of Tables

Chapter 1

Introduction

1.1 Background and Motivation

The dynamics of legged robots with closed-loop mechanisms have been extensively studied in recent years [2, 3, 4, 5, 6, 7]. Those theoretical investigations dealt with the forward dynamics and the inverse dynamics to estimate required actuator torques and forces for the desired motion [8, 9]. The inverse dynamics analysis is highly important for an effective design of the mechanical system inspired from the biological system, in the aim of minimizing the energy consumption and realizing an energy-efficient motion planning. A recent trend is soft robotics and a hybrid design of rigid and soft bodies, which is inspired from soft grounding of running athletes [10, 11, 12, 13] or an appropriate compliance control of walking robots [14, 15, 16, 17] to learn an essence of the muscularskeletal system.

There are several representation of compliant elements by mechanical spring-damper in robotic legged design such as series elastic actuators (SEA) [18], leg design with physical elastic elements [19, 20, 21] inspired from the bi-articular muscle-tendon structure, spring-loaded inverted pendulum (SLIP) model [22], the distal compliance by springy foot [23, 24] as shown in Figure 1-1 (a) may the contributes the reduction of sudden impacts at the point of contact. According to the review by Jie Chen et. al [25], above the mentioned elasticity or compliance in legged system divided into three main categories depending on setting locations and configurations which are

joint series compliance, joint parallel, and leg distal. On the other hand, the effect of elasticity in ground surface during the contact impact process is less considered in robotic foot-ground interaction in comparison with elasticity in the muscularskeletal system. It is necessary to further investigate the implementation and effects of physical damping not only in robotic leg design but also in terms of material properties of ground and leg mechanism as two closed system in contact. In order to study that, one underlying factor is that most damping models will depend on velocity. Therefore, contact force model developed in past decades can be useful to explore the potential functional benefits behind the preferred elasticity in biological systems and to realize a such benefits in design of legged robots. Recently, much attention paid to the less understood behaviour of the adjustable damping tested during the vertical drop with the ground-level perturbations showing that physical damping may help to reject the perturbation by morphological computation, as it mechanically contributes to the rejection of perturbation [26, 27, 28, 29]. The main characteristic of the damping was to reduce unwanted oscillations at touchdown by dissipating the impact kinetic energy of the system by springy components [30]. Hence, we study the effectiveness of physical damping on energy dissipation, to investigate how physical damping can influence the dynamics of the stance phase during the elastic and inelastic contact. We then examine how these predictions relate to driving energy with two different contact cases.

1.2 Towards an understanding the effect of physical damping in legged locomotion

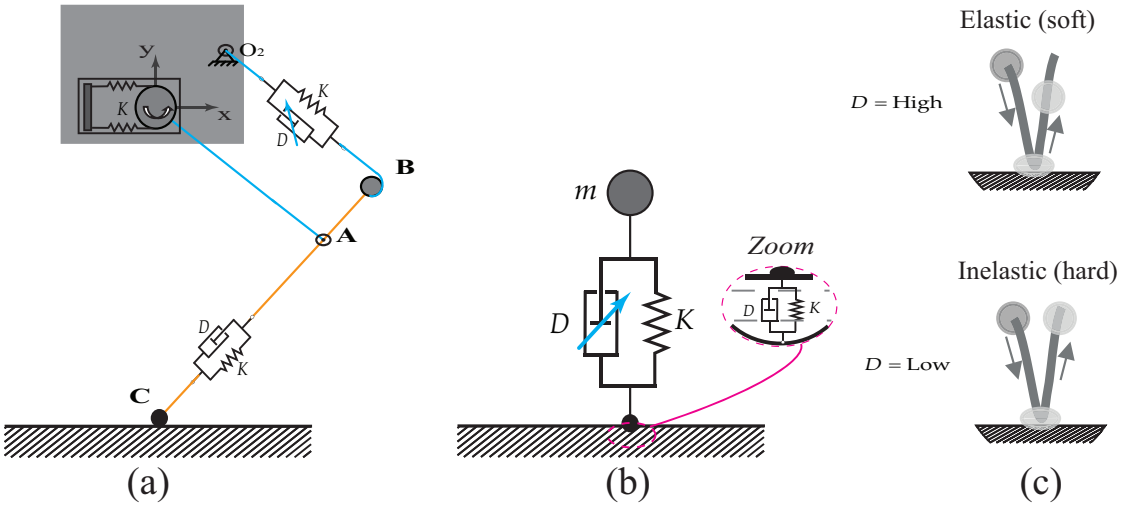

Figure 1-1: Compliant leg model including active and passive elements as well as soft and hard tissues in the system for the case of simple four bar mechanism (a), Mass-spring-damper (MSD) as the simplified model of compliant leg mechanism in general (b), and An effect of the adjustable damping (c).

In the purpose, contact dynamics is significant to model the actual contact process for analyzing an energy dissipation at the moment of the grounding [4, 6]. The computational scheme based on the Lagrangian formulation provides a systematic approach to develop collision and/or sustained contact between rigid bodies, while there are options to focus on either macroscopic or global contact deformations. For binding of methods for the rigid multibody system with the contact dynamics, the formulation based on the non-interpenetration constraints as a unilateral constraint fits to the rigid-body assumption, and then the reaction force from the ground can be estimated with Lagrange multiplier under the constrained predetermined condition [31]. If it is possible to integrate methods for rigid body mechanics and contact dynamics in a consistent manner, the complex muscularskeletal system for walking can be analyzed in a simplification of bodies only with a compliant contact model [32, 33, 34] as shown in Figure 1-1 (b).

1.3 Closed-loop linkage models

In the study by Komoda & Wagatsuma [7] compared different walking mechanisms specifically focusing on the bio-inspired three closed-linkage models and demonstrated an advantage of the model with a smooth grounding of the leg-motion trajectory called the Theo-Jansen mechanism, because of a high energy conservation rather than others. On the other hand, they analyzed a comparison of the energy consumption when moving in the air without considerations of the ground reaction force.

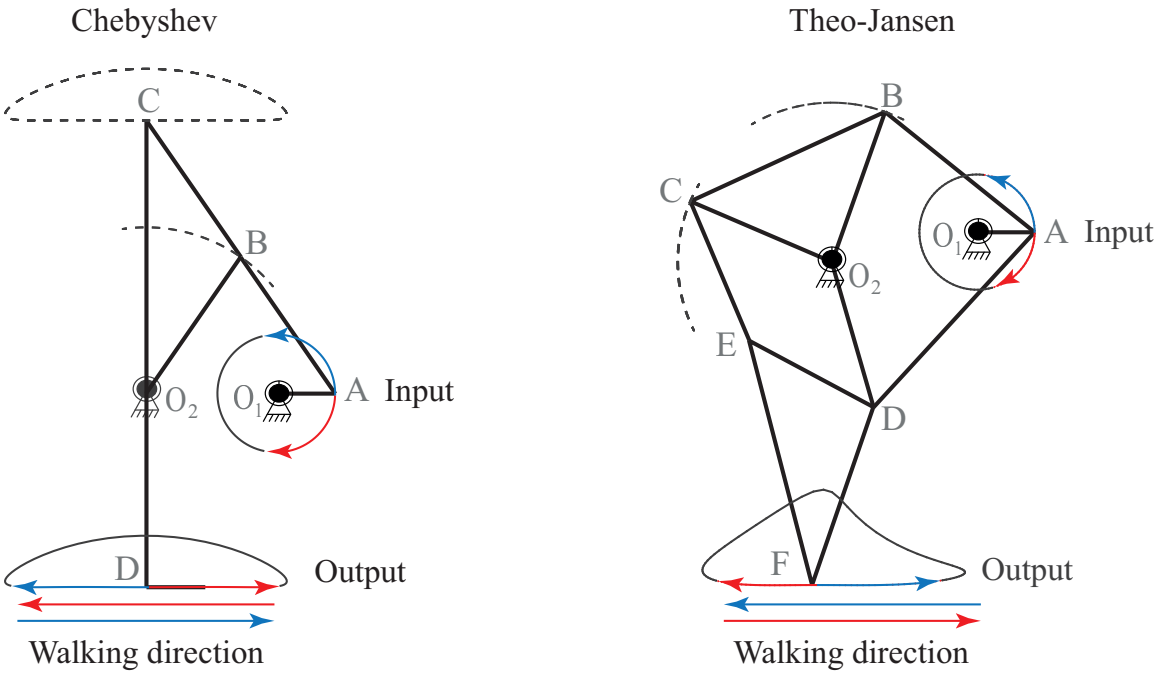

Figure 1-2: The models of typical walking mechanisms with input driving link O_1A and output leg motion. In figure, the arrows represents the direction of rotation of driving link and leg motion associated with driver.

The consideration of impact dynamics when grounding of the leg requires a fine analysis of the forward dynamics of the constrained mechanical system, and the stability of the general solution is required to improve without reducing the number of differential equations to represent the model [35, 36, 37, 38]. Recently, the number of researches was conducted in the modeling of impact analysis in the framework of the multibody system to be able to treat phenomena in collision of elastic bodies. The establishment of the theory of dissipative forces is crucial for viscoelastic

body interactions as discussed by Goldobin et al. [39]. Traditionally, several contact force models for multibody dynamics have been proposed to be generalized contact kinematics, which was extended from pure elastic contact force models to dissipative contact force models [40]. Indeed, the dissipative contact force is more realistic to explain actual phenomena in the outer world for robotic systems to connect, while the formulation requires constitutive laws and damping factors to accommodate the energy dissipation associated with the contact-impact process as illustrated in Figure 1-1 (c). The first dissipative contact force models is considered to be proposed by Kelvin and Voigt [40, 41], which simply assumed a linear relationship between contact force and penetration in deformation, as a first-order approximation. Since the linear spring-damper contact force model does not properly represent the physical nature of the energy transferred between bodies at the contact process as Hunt and Crossley [42] demonstrated, several models were newly proposed to involve the Hertz law as the non-linear equation [39, 40, 43]. Although there are several upgrade versions [40, 44], the most traditional non-linear model is considered to be the model proposed by Lankarani & Nikravesh [45], which successfully integrates the Hertzian contact law associated with a hysteresis damping factor as a continuous contact force model with a high advantage for the contact-impact analysis of multibody systems. Interestingly, in those non-linear viscoelastic models, the contact force can be decomposed into its elastic (conservative) component with the impact spring stiffness parameter and viscous (dissipative) component with the hysteresis damping factor [40]. The hysteresis damping factor controls the amount of hysteresis in the relationship between contact force and penetration in deformation and it includes a critical parameter known as the coefficient of restitution, which determines whether the collision provides completely elastic impact or inelastic impact, by changing the parameter value to be either unity or null [40, 43].

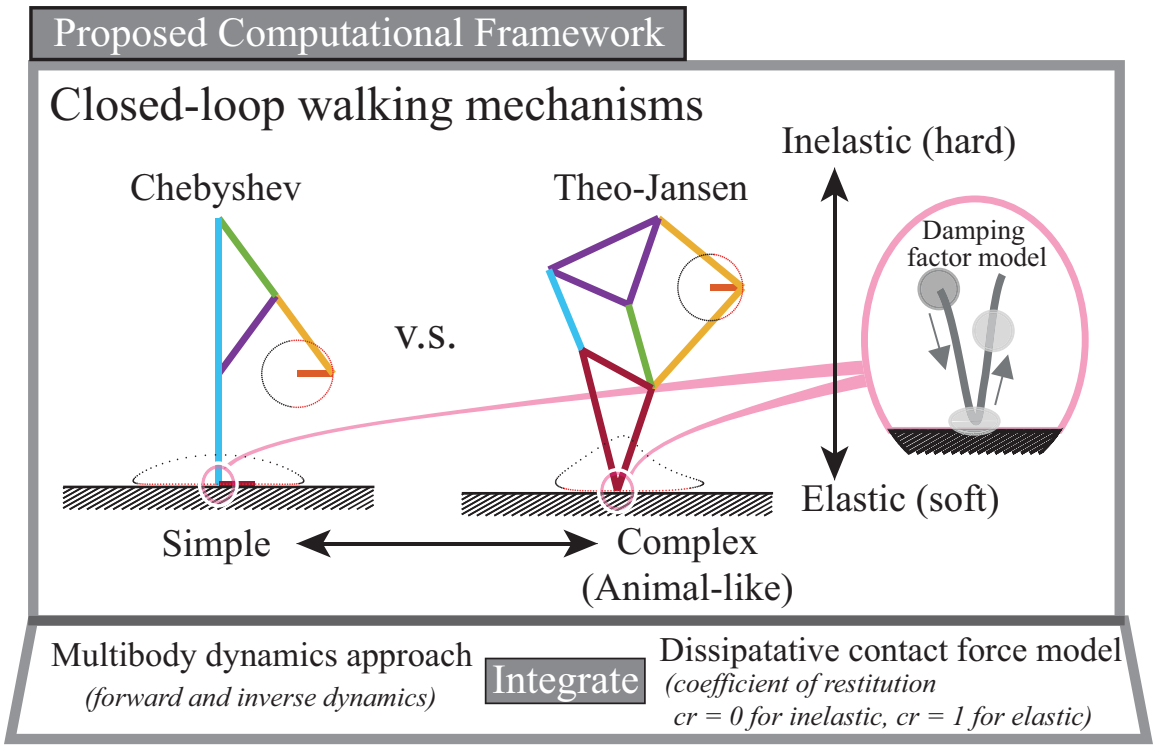

Figure 1-3: Proposed an integrated computational framework

In consideration of robotic systems, particularly in walking mechanisms, a fine contact dynamics model provides a significant benefit to evaluate necessary parameter values to satisfy a desired function. In the passive biped walking robot, called the passive walker, Corral et al. [46] investigated best ranges of coefficients of restitution and friction to realize a sustainable walking motion and successfully visualized the achievement index of walking as a function of coefficients of restitution and friction by using formulations of kinematics and dynamics with the impact dynamics model. Returning to the principle problem in the present study, the establishment of a fine methodology for simulating phenomena of viscoelastic contact with the ground in general example as shown in Figure 1-3 is important for bio-inspired walking mechanisms to prove the efficacy in the energy consumption as an inevitable unsolved problem. As Komoda and Wagatsuma [6] demonstrated, a set of closed-linkage walking mechanisms can be a standard criterion to test the hypothesis that the viscoelastic ground contact contributes to minimizing the energy consumption of walking mechanisms especially in the stance phase, which happing ground reaction forces. For the validation

of the hypothesis, this thesis is devoted to the problem of evaluating required torque of the input driver and the energy consumption of the system with/without viscoelastic effects in cases of Chebyshev and Theo-Jansen mechanisms as typical closed-loop walking mechanisms.

1.4 Organization of this Dissertation

Chapter 2: This chapter, includes the formulation that can be used to analyze the dynamics of planar linkage mechanism within the scope of computational multibody dynamics. The computer algorithms mainly utilized in the dynamic of planar multibody system for the case of forward dynamics analyses are presented. Then, the key aspects related to the dynamic analysis of constrained multibody mechanical systems are discussed for instance, stability of general solution of equation of motion and inverse dynamics of kinematically driven system. The formulation of multibody system dynamics adopted here uses the generalized absolute coordinates to derive the multibody system equations of motion. This formulation results in the establishment of a mixed set of ordinary differential and algebraic equations, which are numerically solved in order to predict the system dynamics.

Chapter 3: In this chapter, some of most relevant contact force models from pure elastic constitutive Hertz law to non-linear dissipative models in contact mechanics are presented. In particular, attention is given to the constitutive law proposed by Lankarani & Nikravesh. The concept of coefficient of restitution in relation to the hysteresis damping factor is derived. The approach presented in this chapter is based on the analysis of energy dissipation associated with the internal damping of the contacting bodies which can be analyzed with various damping factor models proposed by different authors. Furthermore, basic formulation in generalized contact kinematics and its further extension with the framework of multibody system dynamics, are briefly described.

Chapter 4: We introduced a computational framework to integrate the multibody dynamics with dissipative contact force model in simple manner and partially demon-

strated the proposed integrated framework on dynamic analysis of the typical walking mechanism.

Chapter 5: Show demonstrative examples on contact force analysis using proposed integrated method and compared to other existing method. In particular, computational efficiency and numerical accuracy were quantified with simple open-loop and constrained closed-loop system example. Constraint formulation was introduced. The method employ constraint equation to describe the contact between slider-crank mechanism and fixed block. its limitation in larger constrained mechanical system due to poor stability in numerical solution was addressed.

Chapter 6: The rest of the dissertation includes a discussion on the generality and possible application of our method for the analysis of the ground reaction force in animal-like realistic gait trajectories reproduced by the musculoskeletal closed linkage model.

Chapter 7: The limitation of our method associated with the morphological change of the contact surface is stated and possible implementation of the theoretical method dealing with the complex representation of the surface parameter is considered in the future scope of our approach.

Chapter 2

Mathematical formulations in multibody system dynamics

The multibody systems are often very complex and consists of a collection of interconnected rigid and flexible bodies. These bodies are constrained with respect to each other using a set of restrictions. Mathematically, these kinematic pairs (or joints) can be modelled by constraint equations that introduce kinematic relations between the coordinates describing the configuration of mechanical system as shown in Figure 2-1.

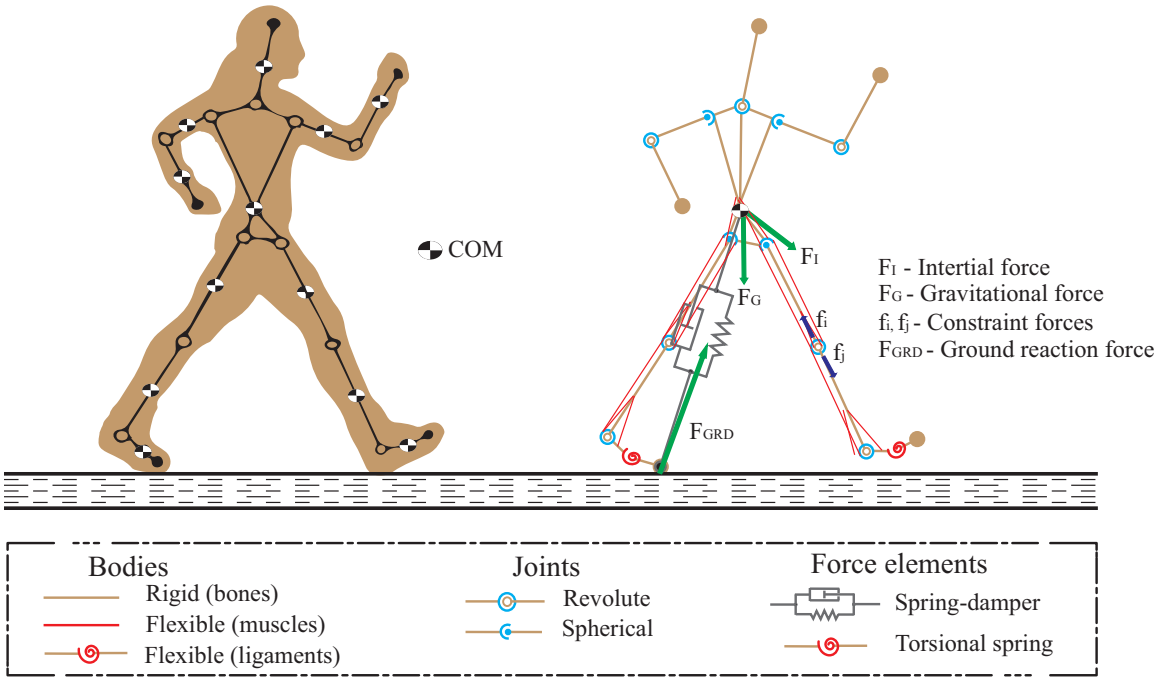

Figure 2-1: Abstract representation of a multibody system with its most significant components bodies, joints, and force elements for the case of human biomechanical model.

The study of kinematics gives information about the motion of a system independently of the forces acting on it. The motion of the system depends on the geometry and configuration of its elements. To understand the kinematics of complex system motion, it is necessary to study the general motion of a multibody system, with emphasis on the restrictions introduced by the kinematic pairs (corresponding to the joints of the linkage system). Therefore, in this section, the systematic computational tools used to determine position, velocity and acceleration of the system are presented. Before going into the detailed description of multibody system formulation, computer and numerical methods to be suitable for implementation on high-speed digital computers based on analytical techniques of Newton, D'Alambert, and Lagrange are introduced in terms of dependent features or factors for the development of computationally efficient computer programs.

Table 2.1: Common techniques dealing with computer simulation of dynamics analysis of multibody system

Existing MBD approaches / Parameters	Augmented formulation	Embedding technique
Structure	Sparse matrix	Matrix
Choice of coordinate system	Absolute Cartesian and Orientation (Body)	Joint coordinates
Stability criteria	Baumgarte method	Coordinate partitioning method
Integrator	Direct integration	
	Runge-Kutta	
Constraint forces	Explicitly appears	Eliminated
Computational efficiency	High	High
Development	General purpose	General or special purpose
Application to the closed loop system	Applicable	Less applicable

There are two basic dynamics formulations which are widely used in computer simulation of multibody systems as shown in Table 2.1. In the augmented formulation, equation of motion expressed in terms of redundant set of coordinates. As result, the constraint forces appear in the final form of equations of motion. An advantage of this formulation is producing simple equations that has sparse matrix structure; therefore, these equations can be solved efficiently even for the complex miltibody system. In the second formulation, constraint forces are eliminated from the dynamic equations by expressing these equations in terms of system degrees of freedom. Which means joint variables often used as the degree of freedom to express the system configuration. its also stated in literature [47] that use of joint variables has the advantage of reducing number of equations and disadvantage of increasing the non-linearity and complexity of equations in case of embedding techniques. Therefore, these type of formulation widely used in the analysis of robot manipulator. The selection of the method is depend on careful consideration of application in our fields for instance, robot manipulator, space structure, and biomechanical systems.

2.1 Formulation for constrained multibody system

The typical walking mechanisms used in this thesis, the anatomical structure are modelled as rigid bodies in closed kinematic chain [48]. Moreover, the multibody

methodology is implemented using absolute Cartesian coordinates. Configuration of the multibody system can be described by an equal number of coordinates defined for each body in the system. The vector of generalized coordinates for the system is written as

$$q_i = \begin{bmatrix} R_i \\ \phi_i \end{bmatrix} = \begin{bmatrix} x_i \\ y_i \\ \phi_i \end{bmatrix} \tag{2.1}$$

where the array of coordinates contains three arrays as $q_i = [x_i, y_i, \phi_i]^T, i = 1, ..., N_b$ for a system of N_b bodies. A set of kinematic constraint equation describing the several commonly used kinematic joints to allow particular relative motion between the adjacent bodies and constraints are expressed by N_b number of absolute coordinates.

2.1.1 Constraint between body and ground

Each rigid body is characterized by a set of points and unit vectors. There are several combinations of points and vectors that can be used when the rigid body is defined. In the presented rigid body linkage model, the number of segment points coincides with the number of body that the element shares with the rest of the chain known as body coordinate formulation. Furthermore, local unit vectors are attached to each body and will be used to determine its absolute orientation. The total number of constraints directly depends on the combination of points and vectors that characterize each segment.

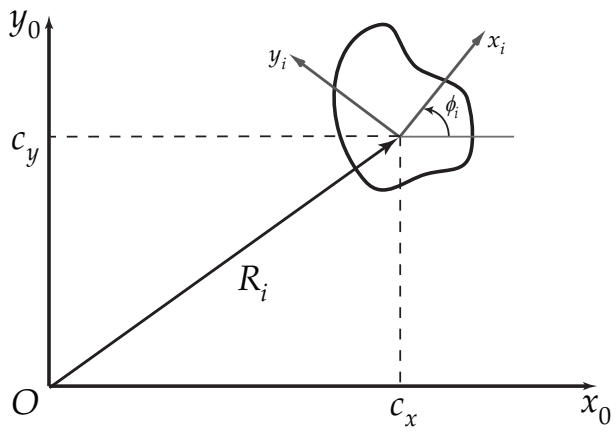

Figure 2-2: Constraints on absolute coordinates of point P_i on body i and angular orientation

Kinematic constraint equations for the absolute position and angular constraint condition as shown in Figure 2-2 can be written as

$$\begin{cases} \Phi^{sx}(q_i) = x_i - c_x \\ \Phi^{sy}(q_i) = x_y - c_y \\ \Phi^{s\phi}(q_i) = \phi_i - c_\phi \end{cases} \tag{2.2}$$

where c_x, c_y, c_ϕ are a given constant. An absolute position constraint on point P_i of body i in x or y direction might be imagined as the condition that pin on body i at point p_i slide in a slot in the x-y plane that is parallel to x or y axis, respectively. In other words, In many mechanical systems, the motion of a body is constrained relative to the ground or fixed on the plane, that is, relative to the stationary frame $x-y$ reference frame as shown in example in Figure 2-2. The use of above mentioned position constraint for the case of closed linkage model is the fixed points or ground nodes O_1 and O_2 in the Chebyshev and the Theo-Jansen linkages, respectively.

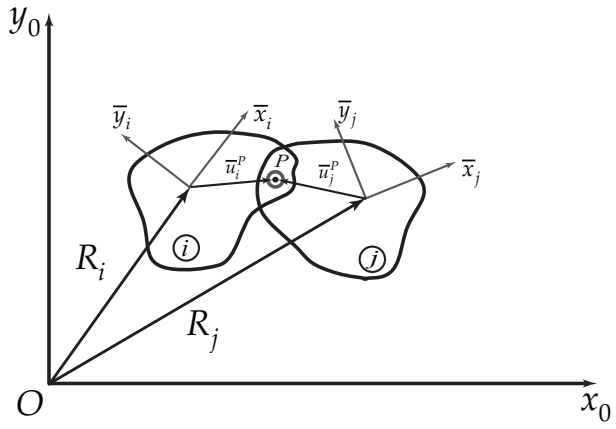

Figure 2-3: Constraints on the revolute joint connecting two body i and j.

One of the frequently used constraint in multibody system is a relative joint that allows relative rotation about the a point P that is common to bodies i and j, as shown in Figure. Physically, such a joint is a rotational bearing between the bodies. This type of joint eliminates the two degrees of freedom from the pair. Constraint equation that define the relative rotational joint can be written as

$$\Phi^{K(i,j)} = r_i^P - r_j^P = (R_i + A_i \bar{u}_i^P) - (R_j - A_j \bar{u}_j^P) \equiv 0 \tag{2.3}$$

where $\bar{u}_i^P$ and $\bar{u}_j^P$ are the unit vector on body i and j, respectively. more explicitly,

$$\Phi^{K(i,j)} = \begin{bmatrix} x_i + \bar{x}_i^P \cos\phi_i - \bar{y}_i^p \sin\phi_i - x_j - \bar{x}_j^P \cos\phi_j + \bar{y}_j^p \sin\phi_j \\ y_i + \bar{x}_i^P \sin\phi_i + \bar{y}_i^p \cos\phi_i - y_j - \bar{x}_j^P \sin\phi_j - \bar{y}_j^p \cos\phi_j \end{bmatrix} = 0 \tag{2.4}$$

where $\Phi^{K(i,j)}$ is describing the kinematic constraint equations on the revolute joints which is obtained by requiring that point P_i and P_j coincide.

2.1.2 Driver constraints

The kinematic constraint presented in section 2.1.1 represent physical connections between bodies; hence they impose limitations on the relative motion between the bodies and with the grounded or fixed node. In addition to the kinematic constraint,

the motion of many mechanical systems is described by actuator input that specifies the time history of some position coordinates or relative position of pair bodies. To uniquely determine the time history of motion of a mechanism, a number of input must be specified, equal in number to the number of degree of freedom of the system. Which is basically specifying the appropriate number of time-dependent driving conditions. A family of standard drivers in multibody system, called driving constraint which are distance driver, rotational driver.

$$\Phi^D(q,t) = [\theta_1 - \omega t] = 0 \tag{2.5}$$

where θ_1 is the initial state of driver constraint and ω is the angular speed. The generalized coordinates describing the system are dependent and several algebraic equations need to be introduced to relate them. Those equations, called kinematic constraint equations, are used in this thesis to guarantee the characteristics of each body (rigid body constraints) Equation (2.4) and also to guide the system motion using rheonomic constraint (driving constraint) Equation (2.5) can be rewritten as

$$\Phi(q,t) = \begin{bmatrix} \Phi^K(q) \\ \Phi^D(q,t) \end{bmatrix} = 0, \tag{2.6}$$

2.1.3 Degree of freedom in constrained mechanical system

For a given examples of closed linkage models, the redundant constraint exists in Equation (2.5) which is described as n_h kinematic constraint equations, the number of degree of freedom is $3N_b - N_h$ degrees of freedom. In general, for the system having N_h independent constraint equations and N_b coordinates, the number of DoF's is obtained as

$$DoF = 3N_b - N_h \tag{2.7}$$

2.2 Forward dynamics approach

In dynamic analysis of mechanical systems, there are two different types of analysis that can be performed, namely, forward and inverse dynamics. For the case of forward dynamics analysis, force that produce motion are given and objective is to determine the position coordinates, velocities, and accelerations. In this type of analysis, acceleration first found from the laws of motion. In most application in closed-form solution is difficult to obtain and, therefore, one must resort to direct numerical integration algorithms. Assuming that the multibody system is consists of constrained bodies or constrained with the ground, the equation of motion must contain reaction forces corresponding to free body diagram (FBD) in order to analyse the dynamics of a system.

$$\begin{cases} M\ddot{q} + \Phi_q^T \lambda = h^{(a)} \\ \Phi(q,t) = 0 \end{cases} \tag{2.8}$$

which is a system of differential algebraic equations (DAE) with n second order ordinary differential equations and with m algebraic constraints. The first derivative of position constraint equation in Equation (2.8) with respect to time is used to obtain the velocity constraint equation while the second derivative of Equation (2.8) with respect to time yields the acceleration constraint equation as

$$\Phi_q \dot{q} = v \tag{2.9}$$

$$\Phi_q \ddot{q} = \gamma \tag{2.10}$$

where Φ_q is the Jacobian matrix of the kinematic constraint equations, v is the velocity equation, and γ is the acceleration equation.

Equation of motion (2.8) and re-written in matrix form expressed in terms of a

redundant set of coordinates as

$$\begin{bmatrix} M & \Phi_q^T \\ \Phi_q & 0 \end{bmatrix} \begin{bmatrix} \ddot{q} \\ \lambda \end{bmatrix} = \begin{bmatrix} h^{(a)} \\ \gamma \end{bmatrix}, \tag{2.11}$$

where M is a system mass matrix, $\ddot{q}$ is the vector that contains the system accelerations. The force acting on the system is known, we integrate the acceleration to determine the velocity. In a forward dynamic analysis, to obtain new coordinates and velocities, two integration array for $\dot{q}$ and $\ddot{q}$ for the time step $t + \Delta t$ is defined

$$u = \begin{bmatrix} q \\ \dot{q} \end{bmatrix}, \quad \dot{u} = \begin{bmatrix} \dot{q} \\ \ddot{q} \end{bmatrix}, \quad \dot{u}(t) \xrightarrow{yields} u(t + \Delta t), \tag{2.12}$$

if the acceleration is known, the velocity and displacement can be found. its clear from the above the equation that one needs give the conditions which are initial velocity and displacement, to be able to integrate the acceleration to determine the displacement and velocity in response to given forces. A system of differential algebraic equations (DAE) with n second order ordinary differential equations and with m algebraic constraints. The strategy to solve these DAE system is based on turning it into an ordinary differential equation (ODE) system, since there are many well-known methods for the integration. The numerical procedure often used for solving the a system of non-linear algebraic equations is the Newton-Raphson algorithm. However, method does not always converge, one must specify an upper limit on the number of iterations used in numerical algorithm. The result of solution of equation of motion is not close enough to the exact solution, an error is made in definition of the system constraint, and/or the multibody system is close to singular configuration [49]. A simple algorithm that can eliminate the need for using Newton-Raphson method is Baumgarte's constraint stabilization method.

2.2.1 Solution of the equation of motion

Above the procedure for forward dynamics analysis requires a set of initial values for coordinates and velocities to start the integration. However, due to the inaccurate initial condition, a time step of the simulation, the accuracy of the numerical integration routine, predicted (approximated) values may not be satisfied with their corresponding constraint with adequate accuracy. Numerical errors due to the finite precision of the numerical methods leads to constraint violation at the coordinate and velocity levels; i.e., $\dot{\mathbf{\Phi}} \neq 0$ and $\mathbf{\Phi} \neq 0$. Therefore, special procedures, capable of eliminating the error in the constraints, or at least keeping such errors under control, should be involved in computational scheme. For the reason, several methods capable of reducing any possibility of constraint violation or at least keeping such errors under given user tolerance were introduced in the past decades, namely constraint stabilization technique [38], and coordinate partitioning method [50]. if there is no error in numerical simulation, constraint must be satisfied with following condition in both position and velocity level as

$$\mathbf{\Phi} \equiv \mathbf{\Phi}(q) \equiv 0, \qquad \dot{\mathbf{\Phi}} \equiv \mathbf{D}v \equiv 0, \tag{2.13}$$

where q is vector of generalized coordinates and $\mathbf{D}$ denotes the system Jacobian matrix and v is the array of generalized velocities. In the computational simulation, numerical error can be obtained as

$$E_{p_i} = \mathbf{\Phi}^T\mathbf{\Phi}, \qquad E_{v_i} = \mathbf{D}v^T\mathbf{D}v \tag{2.14}$$

where index i denote the i-th iteration.

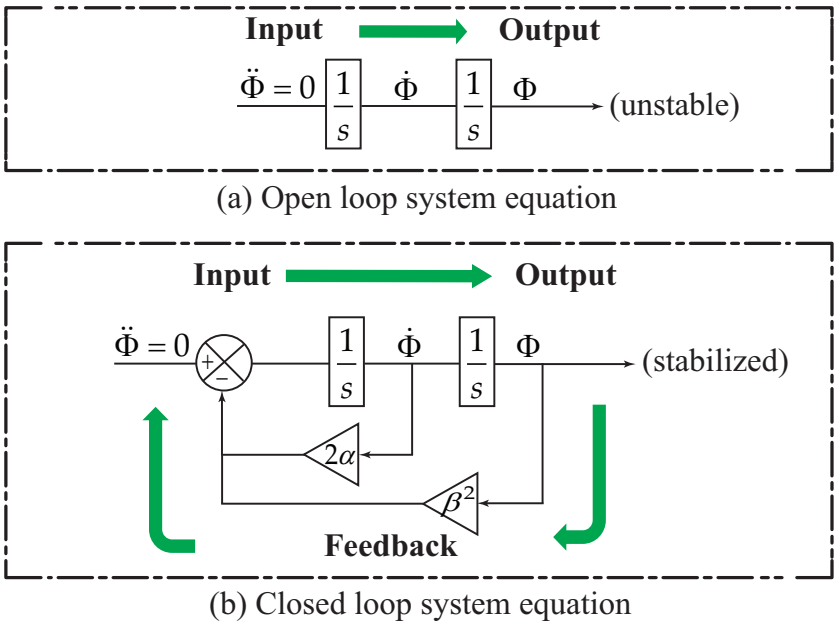

Figure 2-4: Integration methods for the solution of equation of motion. Direct integration (a), Constraint stabilization Baumgarte method (b).

According to the comparative study [37], Baumgarte method, an extension of feedback control theory was presented computationally efficient treatment for the constraint violation, and the simple modification applied to the equation of motion by replacing differential Equation (2.10) employing feedback terms, which contributes to reducing the error at every time step of the simulation is expressed

$$\ddot{\Phi} + 2\alpha\dot{\Phi} + \beta^2\Phi = 0, \tag{2.15}$$

where α and β are positive constants known as compensators. By using the Baumgarte stabilization method, Equation (2.8) becomes

$$\begin{bmatrix} M & \Phi_q^T \\ \Phi_q & 0 \end{bmatrix} \begin{bmatrix} \ddot{q} \\ \lambda \end{bmatrix} = \begin{bmatrix} h^{(a)} \\ \gamma - 2\alpha\dot{\Phi} - \beta^2\Phi \end{bmatrix}, \tag{2.16}$$

The suitable choice of feedback parameters highlighted in the original work by Baumgarte [36] when $\alpha = \beta$, and further investigation by Ostermeyer [35] introduced optimal control system formula to reduce the constraint violation. A systematic de-

termination of parametric study on Baumgarte method was conducted in article by Flores et. al [51]. In addition, the contact force analysis of a multibody system at position and velocity level must be accurate enough to detect instant of contact. Therefore, the integration algorithm not only stabilizes the system value but also provide a variable time-stepping over the period of contact [40].

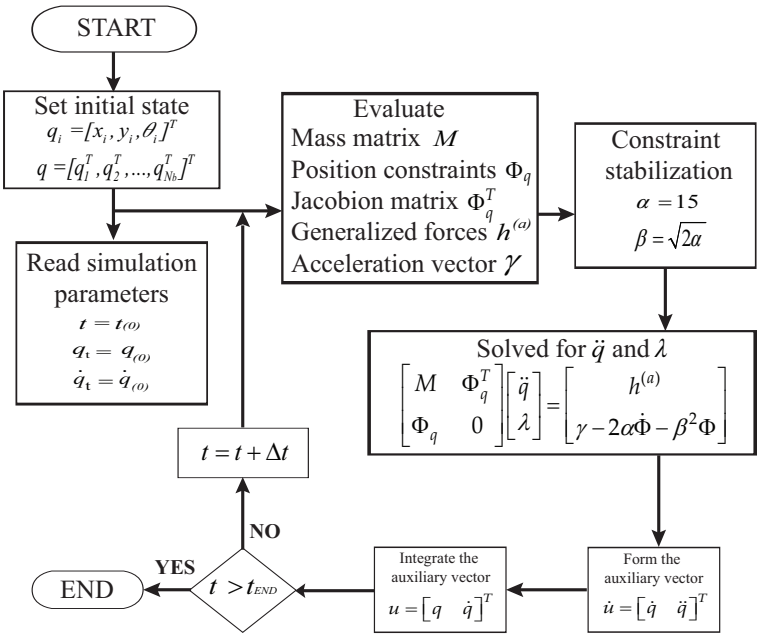

Figure 2-5: Flowchart of iterative procedure for dynamics analysis of multibody systems

if the initial state of the mechanism is given by set of the vector of generalized coordinates on the center of all bodies. The iterative computational procedure as shown in Figure 2-5 can be summarized by the following steps:

1. Start at instant time of $t_{(0)}$ with given initial conditions for position $q_{(0)}$ and velocities $\dot{q}_{(0)}$.

2. Assemble the global mass matrix M, evaluate the Jacobian matrix Φ_q^T, construct the constraint equation corresponding to the joints and restrictions in the closed system, determine the right-hand side acceleration γ and calculate the force vector $h^{(a)}$.

3. Solve the mixed set of differential algebraic equations of motion for acceleration $\ddot{q}$ and Lagrangian multiplier λ at instant t.

4. Assemble the vector $\dot{y}_t$ containing the generalized velocities $\dot{q}$ and accelerations $\ddot{q}$ for instant of time t.

5. Integrate numerically, vector $\dot{q}$ and $\ddot{q}$ with time step $t + \Delta t$ and obtain the new position and velocities.

6. Update the time variable until simulation reach to the end.

2.3 Inverse dynamics approach

Inverse dynamics is widely used in the design and control of many industrial and technological applications, such as robot manipulators and space structures. By specifying the task to be performed by the system, the actuator force and motor torques required to accomplish this task can be predicted. Furthermore, different design alternatives and force configurations can be explored efficiently using the techniques of the inverse dynamics. This is particularly important in modern mechanical system in which some form of control is exerted. An important class of force act in mechanical system is associated with compliant members, such as spring-damper, leaf spring, ground or environmental, and other deformable components that have reaction forces. Force due to compliant members act between the bodies in the system and are functions of relative state variables. Once the acceleration vector is known, the equation of motion described in Equation (2.8) may be solved for λ as

$$M\ddot{q} = h^{(a)} + \Phi_q^{K^T}\lambda^K + \Phi_q^{D^T}\lambda^D \tag{2.17}$$

or equivalently,

$$\begin{bmatrix} \Phi_q^{K^T} & \Phi_q^{D^T} \end{bmatrix} \begin{bmatrix} \lambda^K \\ \lambda^D \end{bmatrix} = M\ddot{q} - h^{(a)} \tag{2.18}$$

where the Lagrange multiplier λ uniquely determines the constraint forces and torque that are acting on the kinematic and driving constraint in the system. This fact motivates the use of terminology inverse dynamics for systems that are kinematically determined. One can estimate the required torque for the desired constraint in the closed system by using Lagrange multiplier. if the driver constraint act on the single coordinate, simplified equation eliminating the Jacobian matrix associated with kinematic constraint was introduced by Nikravesh [9] as

$$\tau = \frac{\dot{\boldsymbol{q}}^T(\boldsymbol{M}\ddot{\boldsymbol{q}} - \boldsymbol{h}^{(a)})}{\dot{\phi}_i}, \tag{2.19}$$

where $\dot{\phi}_i = \omega$ is the velocity of driver constraint, and τ that uniquely determines the load on the driving link.

Finally, the energy consumption was evaluated by the integral of the absolute value of the driving torque, and the angular velocity of the input driver under different loading condition is given as

$$E = \int_{t_0}^{t_1} |\tau\omega| dt. \tag{2.20}$$

Equation (2.17) represents the energy required to drive the mechanism for walking under different loading conditions, which does not include mechanical energy and thermal dissipation at joints.

Chapter 3

Foot-ground contact model

3.1 Kinematic modelling

In general, the motion of a mechanical system is significantly affected by the contact-impact events in the system. Impact is a complex physical phenomenon in which the main characteristics are a small period of time, rapid change in force generation, and large and abrupt changes in the velocities of the contacting bodies as well as material properties should be considered in some application.

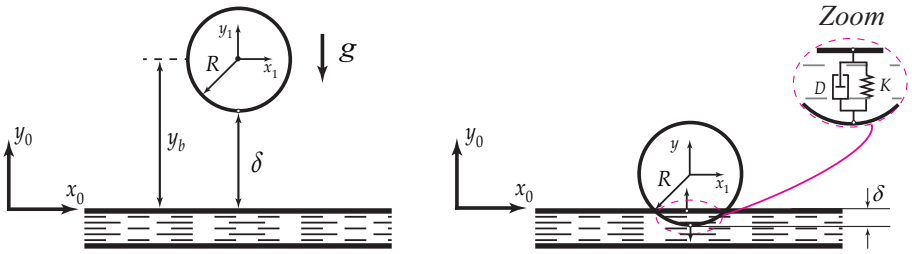

Figure 3-1: Kinematic model representing the contact and non-contact scenario of ball and ground interaction. Non-contact scenario with its kinematic components (a), Contact scenario with Spring-damper model representing the elastic impact in normal direction.

$$\delta = y_b - R \tag{3.1}$$

where y_b is the distance between ball center and ground and R represents the radius of the ball. This is the most simple form of equation describing the contact kinematics and can be applied to the determination of walking phase analysis of the typical walking mechanisms used in this thesis. In previous study by Komoda and Wagatsuma [7] introduced a curvature analysis, in the view point of well-designed fixed end-trajectory reproduced by traditional linkages, method is efficient to determine the edges then the representative two points were commonly used for the definition of the stance phase to obtain the start and end points in the stride. They also mentioned that function of differentials, does not exactly determine the turning points appearing in the numerical solution because there exists a zero-length loop. Therefore, the method may not be applicable in general case if complexity of trajectory and ground surface are increased. Another example by author of Moreira et.al [52] presented a mathematical model for foot ground surfaces in biomechanical multibody system. Model represent the possible integration of penetration model of contact mechanics and general procedure of kinematic configuration (global coordinates, inertial reference frames) in miltibody system.

In a simplest manner, a contact mechanics problem occurs when two bodies that are initially come into contact as shown in Figure 3-1 Contact kinematics of simple ball and ground interaction is to explain the determination of the contact force as function of penetration between the contacting bodies can be formulated as

$$\delta = \begin{cases} \delta & (\delta_N \geq 0 \quad F_N = 0) \\ -\delta & (\delta_N \leq 0 \quad F_N \geq 0) \end{cases} \tag{3.2}$$

In equation (3.2), the positive value of δ is that distance represent a separation, while negative values denote relative deformation or penetration of the contacting bodies. These two scenarios are illustrated in Figure 3-1 (a) and (b), respectively. Therefore, the sign of penetration indicates the transition from separation to in contact and vice versa. The evaluation of the contact kinematics involves the calculation of three essential quantities, namely the position of the potential contact points P_n, relative distance δ and velocity $\dot{\delta}$ in normal and tangential direction.

3.2 Formulations for contact impact analysis

An equivalent system of the contact process between the solid sphere and fixed unmoving box or ground is considered to get the relationship between the deformation and contact force. As shown in Figure 3-2, δ_m, and t_1 to t_5, are maximum deformation and timing, respectively. In this model, two phases, the compression phase and the restitution phase, are included during the impact process. During the compression phase, the indentation deformation δ increases from zero to the maximum compression deformation δ_m, and the initial contact force reaches at maximum value F_{max}.

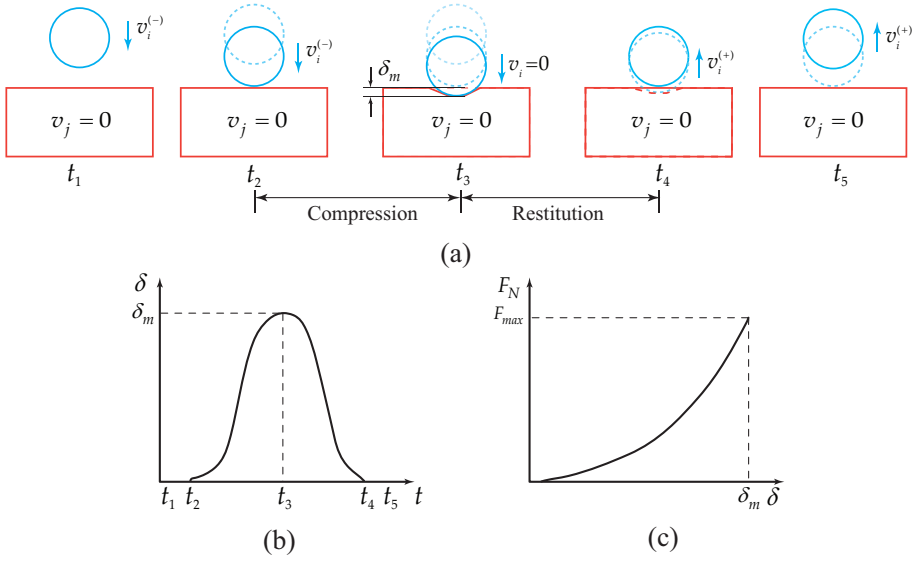

Figure 3-2: Representation of the one-dimensional direct central-impact between ball and ground (a), dynamic response of contact impact event: deformation at instant time (b), elastic component of the contact force versus deformation (c).

The most popular contact force model by Hertz on contact problems has remained an important basis for both fundamental research and engineering application of contact mechanics until now. Based on the elastic mechanics, Hertz model described the relationship between the normal contact force F_N and the non-linear power function of penetration depth δ is expressed as

$$F_N = K\delta^n \tag{3.3}$$

where K represents the stiffness of contacting bodies and δ is the penetration caused by deformation, as illustrated in Figure 3-1 (a). For contact between other technically relevant shapes sphere, cube, prism, cylinder(horizontal and vertical), cone and ground the exponent n can be estimated according to Popov [53].

3.2.1 Modeling of normal contact force

A fundamental problem on the contact force model concerning the loss of energy is firstly considered by Goldsmith [41]. As well as the investigation by Hunt and Crossley [42], the model accounts for the energy dissipation by applying non-linear viscous-elastic element, which can be expressed as

$$F_N = K\delta^n + D\dot{\delta}, \tag{3.4}$$

where K, D and δ denote respectively a generalized stiffness parameter, the damping coefficient and the same relative penetration or indentation[40]. Exponent n is equal to $3/2$ for the case as a parabolic distribution of contact stresses for isotropic material, which was developed by Herts [54] based on the theory of elasticity. The second term represents viscous (dissipative) components concerning the penetration velocity at the start of the firmness and at the end of the compensation evaluated with D as a function of penetration as

$$D = \chi\delta^n, \tag{3.5}$$

where χ is the hysteresis damping factor in terms of the coefficient of restitution as

$$\chi = \frac{3K(1-c_r)}{2\dot{\delta}^{(-)}}, \tag{3.6}$$

where c_r denotes the coefficient of restitution. It is defined as

$$c_r = \frac{\dot{\delta}^{(+)}}{\dot{\delta}^{(-)}}, \tag{3.7}$$

where $\delta^{(-)}$ and $\delta^{(+)}$ denotes respectively the relative approach and relative departing velocities. If purely elastic contact occurs, e = 1, the hysteresis damping factor equals to zero; if the contact is purely plastic, that is, e = 0, the hysteresis damping factor tends to be infinite from the view of physics. Finally, the normal contact force in conjunction with the hysteresis damping factor may be described in an alternative form. Substitution of Equation (3.5) into Equation (3.4) delivers the following form of the normal contact force model:

$$F_N = K\delta^n \left[1 + \frac{3(1-c_r)}{2}\frac{\dot{\delta}}{\dot{\delta}^{(-)}}\right]. \tag{3.8}$$

The damping factor in Equation (3.5) is reviewed on the amount of contact force for conditions whether c_r closer to 1 or closer to 0 [55, 45]. Flores et al. [55] model is suitable for the computational purpose with considerations of the stored elastic energy and dissipated energy associated with internal damping. The damping factor becomes infinity when $c_r = 0$ and then the model provides a non-negligible larger force than the model proposed by Lankarani & Nikravesh [45]. In the model, the perfectly inelastic contact is observed based on hysteresis damping factor as a function of restitution for different contact force models presented in comparative analysis [56, 57].

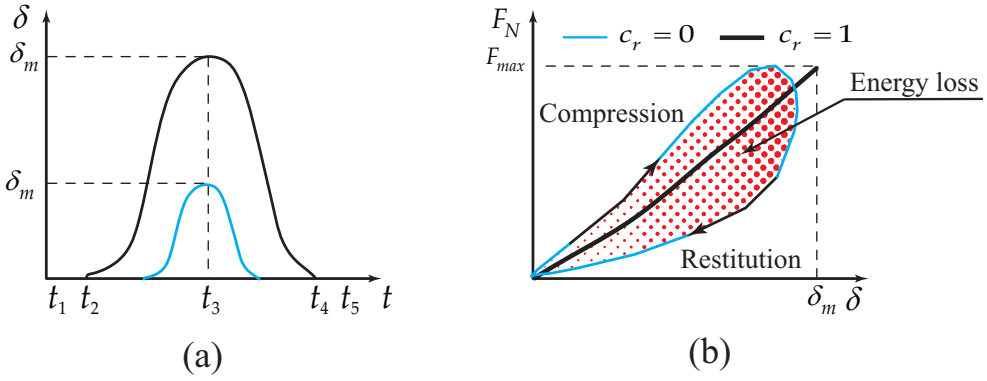

Figure 3-3: Influence of the coefficient of restitution c_r on the ball-ground interaction. Deformation at instant time (b), viscoelastic behaviour (c).

In order to understand the effect of the coefficient of restitution c_r, the dynamic response of the is presented in Figure 3-3 , contact force is plotted against deformation.

In these case of studies presented here, two different values for coefficient of restitution are selected as unity and null. As it expected when coefficient of restitution decreases, maximum deformation and the maximum contact force values are reduced. This is indicated by the increase of contact duration and size of hysteresis loop associated with energy dissipated during the contact process as shown in Figure 3-3 (b). its also shown that coefficient of restitution equal to unity, there is no energy dissipation in contact process correspond to the pure elastic Hertz contact law as presented in Equation (3.1) and Figure 3-2

Equation (3.7) suggests that the shape of the hysteresis loop as shown in Figure 3-3 (b) and the solution corresponding to the variations of the indentation would depend on different parameters such as the the ratio of relative approach and departing velocities of the two body formulated as coefficient of restitution. Thus, the contact force model [45] was introduced in the present study by using the coefficient of restitution $c_r = 0$ as an inelastic (or plastic) contact, resulting in a maximum loss of kinetic energy due to the internal damping is relatively smaller for the purpose as

$$F_N = K\delta^n \left[1 + \frac{3(1-c_r^2)}{4}\frac{\dot{\delta}}{\dot{\delta}^{(-)}}\right]. \tag{3.9}$$

The equation is valid in assumptions that contacting velocities are lower than the propagation speed of elastic waves across two bodies, *i.e.* $\dot{\delta}^{(-)} \leq 10^{-5}\sqrt{E/\rho}$, where E is Young's modulus and ρ is the material mass density. A recent proposal by Ghorbani et al. [58] can be considered in the further investigation under the assumption that the proper drop impact velocity could be determined to reach a required spreading factor examined by dissipative particle dynamics simulations.

3.2.2 Modeling of tangential friction force

A friction model is considered between two bodies of different shapes as contacting surfaces. The dynamic friction forces F_f in the presence of sliding [59, 60] can be expressed as

$$F_f = -\mu F_N c_f c_d. \tag{3.10}$$

where μ the kinetic friction coefficient. In order to take the friction force effect into account with respect to the modified Coulomb law, the direction of the tangential velocity vector $c_f = |v_T|$ with the target body velocity v_T, which is opposite to direction of motion. c_d is the dynamic correction coefficient derived from v_T and the upper limit v_0 and lower limit v_1 of the friction velocity as

$$c_d = \begin{cases} 0 & v_T \leq v_0 \\ (v_T - v_0)/(v_1 - v_0) & v_0 \leq v_T \leq v_1. \\ 1 & v_T \geq v_1 \end{cases} \tag{3.11}$$

It implies that the friction force disappears in either way it is close to zero velocity or there is no contact has been discussed in the context of one-dimensional friction models [61]. If the normal force F_N is obtained from a contact with a force-deformation (Equation (3.9)), a logical point-to-point spring-damper element [8, 9] is only active during the period of contact, and the friction force could be categorized as an applied force due to no explicit constraints to be an interaction between the ground and a leg. When the contact is modeled as kinematic joints (or constraints), a coefficient of Lagrangian represents the resulting contact force, and the corresponding friction could be categorized as a reaction force [62]. In our analysis, the ground reaction force was estimated as unknown applied force from the ground in the stance phase according to the compliant contact force model defined as

$$\boldsymbol{M}\ddot{\boldsymbol{q}} + \boldsymbol{\Phi}_{\boldsymbol{q}}^T \boldsymbol{\lambda} = \boldsymbol{h}^{(a)} + \boldsymbol{h}^{(GRF)}, \tag{3.12}$$

where $\boldsymbol{h}^{(GRF)}$ is the external (ground) reaction force and the total force acting on the point of contact during the stance phase is $\boldsymbol{h}^{(a)} + \boldsymbol{h}^{(GRF)} = \begin{bmatrix} F_f, & -m_i g + F_N, & 0 \end{bmatrix}^T$. If there are no applied forces except the gravitation, such as the swing phase, equations of motion is given as

$$\boldsymbol{M}\ddot{\boldsymbol{q}} + \boldsymbol{\Phi}_{\boldsymbol{q}}^T \boldsymbol{\lambda} = \boldsymbol{h}^{(a)}, \tag{3.13}$$

where the constrained segment of dynamics is accompanied with the generalized force vector $\boldsymbol{h}^{(a)} = [0, \ -m_1 g, \ 0, ..., 0 \ -m_i g, \ 0]^T$ in which m_i is the mass of the body (i), and g is the gravitational acceleration.

Chapter 4

An integrated computational framework for the energy analysis of rigid closed-loop walking mechanisms

In this chapter we integrate the formulations presented in Chapter 2 and 3 of computational procedure of the constrained multibody system and the compliant contact force in one computational. Graphical representation of computational procedure is shown in Figure 4-1. At the starting point of the numerical simulation, initial configurations of target mechanisms are given according to the primary operation in the forward dynamics analysis. For the contact force analysis, the type of collision given by coefficients of restitution in the range from 0 to 1 is an option as the initial parameter of the framework.

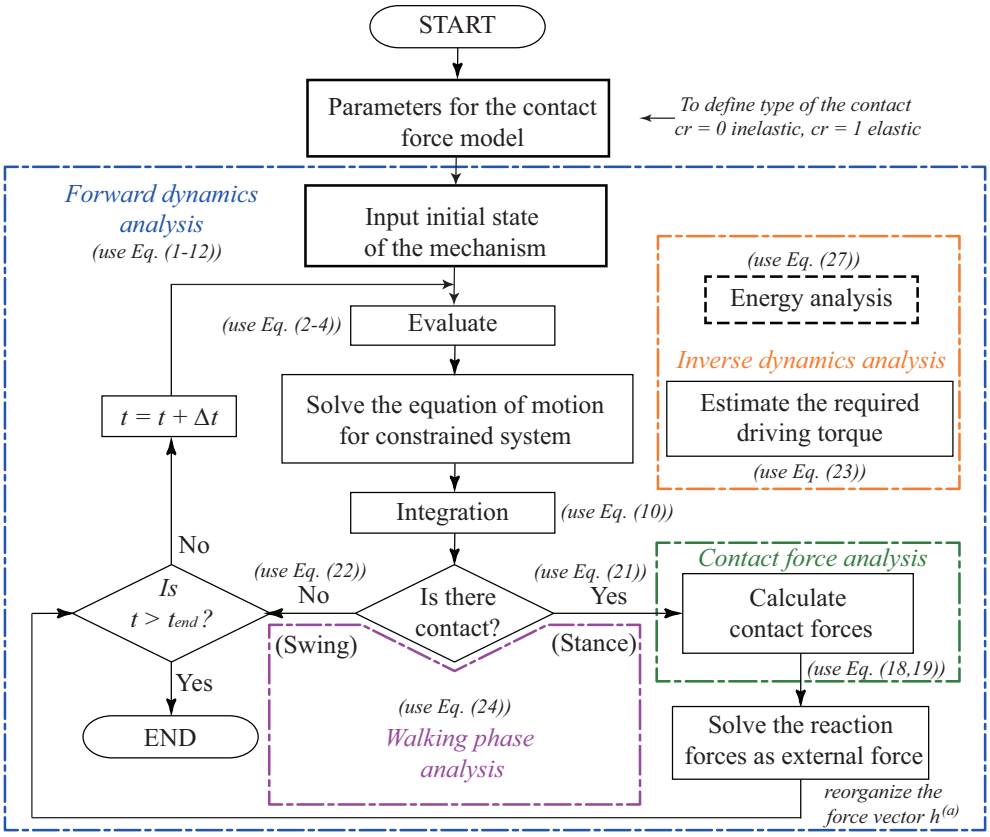

Figure 4-1: An integrated computational framework to be able to evaluate the energy conservation effect in a viscoelastic ground contact in cases of closed-loop walking mechanisms.

The simulation procedure for the proposed computational framework as shown in Figure 4-1 can be summarized by the following steps:

1. Start at instant time $t_{(0)}$ with given initial configuration of the mechanisms such as generalized coordinates defining the position and orientation of each body.

2. Define the initial parameters for the contact force analysis such as contact stiffness K, kinetic frictional coefficient μ, and other necessary variables.

3. Input the type of contact by digits from 0 to 1, inelastic to elastic, respectively.

4. Assemble the global mass matrix M, evaluate the Jacobian matrix Φ_q^T, construct the constraint equation corresponding to the joints and restrictions in the closed system, determine the right-hand side acceleration γ and calculate the force vector $h(a)$.

5. Solve the mixed set of differential algebraic equations of motion for acceleration $\ddot{q}$ and Lagrangian multiplier λ at instant t.

6. Integrate numerically, vector $\dot{q}$ and $\ddot{q}$ with time step $t + \Delta t$ and obtain the new position and velocities.

7. Estimate the relative position between potential contact point P_n of leg mechanism and ground plane y_G at instant time t.

8. Check for contact between leg mechanism and ground and: (i) if no new contact is detected, update the time and proceed step 9 of this procedure; (ii) if there is a contact occurs, calculate the contact reaction forces in normal and tangential direction and reorganize the generalized force vector $h^{(a)}$ by applying the ground reaction force as external applied force h^{GRF} at the during the period of contact.

9. Update the time variable and go to the step 4 if the current time of analysis is smaller than the end time of simulation. Otherwise terminate the analysis.

4.1 Kinematics and gait trajectory analysis

According to the multibody dynamics (MBD) formulation above, the constitutive contact force model is calculated numerically with kinematic and dynamic analyses, which allow to visualize temporal evolutions of the leg-motion trajectory, velocity and acceleration.

Table 4.1: Parameters used in the numerical simulation

Kinematic/Dynamic analysis			Contact force analysis		
Gravitational acceleration $[m/s^2]$	g	9.81	Stiffness $[N/m]$	K	2×10^4
The velocity of the driving crank $[rad/s]$	ω	2π	Coefficient of restitution	cr	$0 \leq cr \leq 1$
Total simulation time $[s]$	t	$0 \leq t \leq 3$	Coefficient of kinetic friction	μ_k	0.4
Baumgarte parameters	α	15			
Baumgarte parameters	β	$\sqrt{2\alpha}$			
Time step $[s]$	dt	1×10^{-3}			

Parameters in Table 4.1 were used for the numerical simulation for dynamic analyses of two closed-loop walking mechanisms. MATLAB-based numerical simulation was performed with a combination of the Euler method with the time step of 1.0×10^{-3}s. In order to reduce an accumulation numerical error, Baumgarte method [35, 36] was introduced with feedback parameters for the stability of the general solution in equations of motion. For the contact analysis to prevent an unnatural rise of ground reaction force, the stiffness was determined with a criterion value as 2×10^4 N/m for contacting bodies according to the work of Ristow [63]. Thus, the ground deformation is equivalent to the resultant motion of the stiffness-damping system under the compression.

Table 4.2: Parameters of each link length (m) and mass (kg)

Chebyshev				**Theo-Jansen**			
Link	Side	Length	Mass	Link	Side	Length	Mass
l_1	O_1A	0.100	0.025	l_1	O_1A	0.100	0.025
l_2	AB	0.282	0.071	l_2	AB	0.333	0.083
l_3	O_2B	0.282	0.071	l_3	O_2B	0.277	0.069
l_4	BC	0.282	0.071	l_4	BC	0.372	0.093
l_5	CD	0.793	0.198	l_5	O_2C	0.267	0.067
l_6	DE	0.050	0.013	l_6	AD	0.413	0.103
a	O_1O_2	0.222	-	l_7	O_2D	0.262	0.066
				l_8	CE	0.263	0.066
				l_9	DE	0.245	0.061
				l_{10}	DF	0.327	0.082
				l_{11}	EF	0.438	0.110
				a	O_1O_2	0.257	-

For the consistent comparison [7], each length and mass of individual links are determined from the normalization based on the equivalent size of driving crank O_1A

as the radius of 0.1 m in two mechanisms as shown in Table 4.2. The number of links is different depending on each mechanism, *i.e.* Chebyshev has five links and the Theo-Jansen mechanism has eleven links.

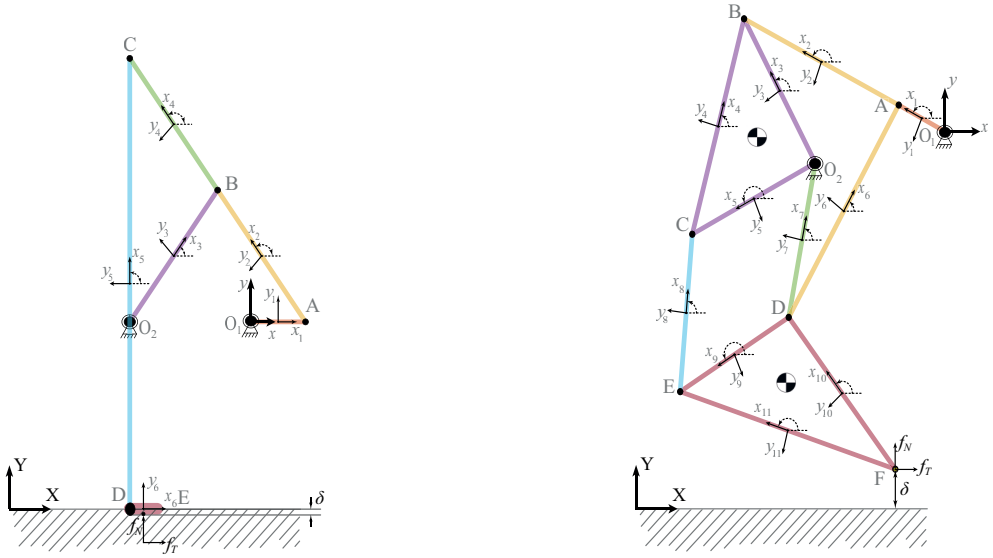

Figure 4-2: Representations of foot-ground interactions by kinematic models of two walking mechanisms. (a) Result in the Chebyshev mechanism and (b) result in the Theo-Jansen mechanism.

Contact and non-contact scenarios were considered in the kinematic model according to penetration equation presented in Chapter 3, as shown in Figure 4-2. When the leg contacts with the ground, the deformation or penetration is estimated as

$$\delta = y_G - P_n, \tag{4.1}$$

where the P_n is the normal component of the position vector or the potential contact point, as $E = [E_x, E_y]$ and $F = [F_x, F_y]$ respectively for Chebyshev and Theo-Jansen mechanisms. The ground plane y_G is consistently leveled from the lowest point of the leg-motion trajectory in the sense of the relative indentation. Negative values of δ means the bodies are in contact. Therefore, the sign of penetration indicates the phase transition from swing to stance and vice versa. By using Equation (4.1), it is clear to discriminate a walking phase and determine contact forces from the function

of penetration.

4.1.1 Formulation for Chebyshev mechanism

Chebyshev mechanism as shown in 4-2(a), the length of all links and grounded node O_1 and O_2 were tightly fixed according to the geometric equations [64]. Simply explaining the working principle of closed-loop mechanism, the leg motion is generated by the links in the system, namely, two fixed nodes O_1 and O_2, three links with the same length, which are $AB = O_2B = BC$ and the input driver of rotating crank O_1A. The rocker links connecting the point O_2 to B follows the motion of the connecting rod and rotating crank. The extension link CD projects from a loop trajectory at the top onto the bottom as known Chebyshev plantigrade [64] (see Figure 4-3). In the operation of this plantigrade machine, movements of the extension link are restricted by another pair legs where it connects with 90 degrees at the input driver and its relative rotational motion is modified. Thus, the mechanism has the translational motion at the foot-link CDE as the desired ideal walking pattern with few numbers of links. The kinematic model for the Chebyshev mechanism is illustrated in 4-2(a), the vector q with 18 elements including position and orientation of each body in leg mechanism expressed as generalized coordinates as follows:

$$\mathbf{q} = [q_1^T, q_2^T, q_3^T, q_4^T, q_5^T, q_6^T]^T \tag{4.2}$$

The vector of q contains $18(= 63)$ elements which are 6 rigid links and their center of position x_i, y_i and orientation ϕ_i are obtained in the generalized coordinates in the present analysis. A set of kinematic algebraic constraint equation according to the initial configuration for the position analysis can be written

$$\mathbf{\Phi}(\mathbf{q},t)=\begin{bmatrix}\Phi^K(q)\\ \Phi^D(q,t)\end{bmatrix}=\begin{bmatrix}x_1-l_1cos\theta_1\\ y_1-l_1sin\theta_1\\ x_2-l_2cos\theta_2-x_1-l_1cos\theta_1\\ y_2-l_2sin\theta_2-y_1-l_1sin\theta_1\\ x_3+l_3cos\theta_3-x_2-l_2cos\theta_2\\ y_3+l_3sin\theta_3-y_2-l_2sin\theta_2\\ x_3-l_3cos\theta_3+a\\ y_3-l_3sin\theta_3\\ x_4-l_4cos\theta_4-x_2-l_2cos\theta_2\\ y_4-l_4sin\theta_4-y_2-l_2sin\theta_2\\ x_5+l_5cos\theta_5-x_4-l_4cos\theta_4\\ y_5+l_5sin\theta_5-y_4-l_4sin\theta_4\\ x_6-l_6cos\theta_6-x_5+l_5cos\theta_5\\ y_6-l_6sin\theta_6-y_5+l_5sin\theta_5\\ \theta_4-\theta_2\\ \theta_5-\frac{\pi}{2}\\ \theta_6-\theta_6\\ \theta_1+\omega t\end{bmatrix}_{18\times1}=\mathbf{0} \tag{4.3}$$

where the first 17 elements of the column matrix $\Phi^K(q)$ are derived from Equation (2.5) for absolute constraints between body and ground, and Equation (2.4) for constraint equation for revolute joins connecting the rigid links. The last element $\Phi^D(q,t)$ is derived by the driving constraint Equation (2.6).

The partial derivative of position constraint equation respect to the generalized absolute cartesian coordinates q is Jacobian matrix $\mathbf{\Phi}_q$ is obtained as:

$$\mathbf{\Phi}_q=\left[\frac{\partial\mathbf{\Phi}(\mathbf{q},t)}{\partial\mathbf{q}}\right]_{18\times18}, \tag{4.4}$$

where it allows us to investigate placement, velocity and acceleration analyses kinematically. The forward dynamics analysis introduces the mass matrix $\mathbf{M}(18\times18)$, and the generalized external force vector $\mathbf{h^a}(18\times1)$, as follows:

$$\mathbf{M}=diag(M_1,M_2,\cdots,M_6), \tag{4.5}$$

$$\{\mathbf{M}_i=[m_i,m_i,J_i]^T\mid i=1,2,\cdots,6\}, \tag{4.6}$$

$$\mathbf{h^{(a)}}=[h_1^{(a)^T},h_2^{(a)^T},\cdots,h_6^{(a)^T}]^T, \tag{4.7}$$

$$\{\mathbf{h^{(a)}}_i=[0,-m_ig,0]^T\mid i=1,2,\cdots,6\}, \tag{4.8}$$

where m_i is the mass of rigid linkage to point i, $J_i = 2l_i/3$ is the polar moment of inertia of rigid linkage to point i, and g is the gravitational acceleration.

4.1.2 Formulation for Theo-Jansen mechanism

The Theo-Jansen mechanism [65] has multiple geometrical structures coupled into the closed chain system and it produces relative rotational and translational motions at the foot-link as shown in Figure 4-2(b). It consists of a pair of identical upper four-bar linkage O_1ABO_2 with a coupler (rigid triangle) O_2BC and lower four-bar linkage O_1ADO_2. DEF connection resembles a rigid foot-link since the relative angle between them is a constant, which eliminates all three-relative degrees of freedom. In the working principle, each four-bar forms a stiff triangle as a parallelogram, and the rectangle $CEDO_2$ changes its shape and regulates the motion of the foot-end point F. The kinematic model for the Theo-Jansen mechanism, the vector q with 18 elements including position and orientation of each body in leg mechanism expressed as generalized coordinates as follows:

$$\mathbf{q} = [q_1^T, q_2^T, q_3^T, q_4^T, q_5^T, q_6^T, q_7^T, q_8^T, q_9^T, q_{10}^T, q_{11}^T]^T \tag{4.9}$$

The vector of q contains 33 ($= 11 \times 3$) elements which are 11 rigid links and their center of position x_i, y_i and orientation ϕ_i are obtained in the generalized coordinates in the present analysis. A set of kinematic algebraic constraint equation according to the initial configuration for the position analysis can be written

$$\mathbf{\Phi}(\mathbf{q},t) = \begin{bmatrix} \Phi^K(q) \\ \Phi^D(q,t) \end{bmatrix} = \begin{bmatrix} x_1 - l_1 cos\theta_1 \\ y_1 - l_1 sin\theta_1 \\ x_2 - l_2 cos\theta_2 - x_1 - l_1 cos\theta_1 \\ y_2 - l_2 sin\theta_2 - y_1 - l_1 sin\theta_1 \\ x_3 + l_3 cos\theta_3 - x_2 - l_2 cos\theta_2 \\ y_3 + l_3 sin\theta_3 - y_2 - l_2 sin\theta_2 \\ x_3 - l_3 cos\theta_3 - a_x \\ y_3 - l_3 sin\theta_3 - a_y \\ x_5 + l_5 cos\theta_5 - x_4 + l_4 cos\theta_4 \\ y_5 + l_5 sin\theta_5 - y_4 + l_4 sin\theta_4 \\ x_7 - l_7 cos\theta_7 - x_6 + l_6 cos\theta_6 \\ y_7 - l_7 sin\theta_7 - y_6 + l_6 sin\theta_6 \\ x_9 + l_9 cos\theta_9 - x_8 + l_8 cos\theta_8 \\ y_9 + l_9 sin\theta_9 - y_8 + l_8 sin\theta_8 \\ x_{11} - l_{11} cos\theta_{11} - x_{10} + l_{10} cos\theta_{10} \\ y_{11} - l_{11} sin\theta_{11} - y_{10} + l_{10} sin\theta_{10} \\ x_6 + l_6 cos\theta_6 - x_1 - l_1 cos\theta_1 \\ y_6 + l_6 sin\theta_6 - y_1 - l_1 sin\theta_1 \\ x_4 + l_4 cos\theta_4 - x_2 - l_2 cos\theta_2 \\ y_4 + l_4 sin\theta_4 - y_2 - l_2 sin\theta_2 \\ x_5 - l_5 cos\theta_5 - a_x \\ y_5 - l_5 sin\theta_5 - a_y \\ x_7 + l_7 cos\theta_7 - a_x \\ y_7 + l_7 sin\theta_7 - a_y \\ x_8 + l_8 cos\theta_8 - x_4 + l_4 cos\theta_4 \\ y_8 + l_8 sin\theta_8 - y_4 + l_4 sin\theta_4 \\ x_9 - l_9 cos\theta_9 - x_6 + l_6 cos\theta_6 \\ y_9 - l_9 sin\theta_9 - y_6 + l_6 sin\theta_6 \\ x_{10} + l_{10} cos\theta_{10} - x_6 + l_6 cos\theta_6 \\ y_{10} + l_{10} sin\theta_{10} - y_6 + l_6 sin\theta_6 \\ x_{11} + l_{11} cos\theta_{11} - x_8 + l_8 cos\theta_8 \\ y_{11} + l_{11} sin\theta_{11} - y_8 + l_8 sin\theta_8 \\ \theta_1 + \omega t \end{bmatrix}_{33\times 1} = \mathbf{0} \tag{4.10}$$

where the first 32 elements of the column matrix $\Phi^K(q)$ are derived from Equation (2.5) for absolute constraints between body and ground, and Equation (2.4) for constraint equation for revolute joins connecting the rigid links. The last element $\Phi^D(q,t)$ is derived by the driving constraint Equation (2.6). The Jacobian matrix for Theo-Jansen mechanism $\mathbf{\Phi}_q$ is obtained as:

$$\mathbf{\Phi}_q = \left[\frac{\partial \mathbf{\Phi}(\mathbf{q},t)}{\partial \mathbf{q}} \right]_{33\times 33}, \tag{4.11}$$

where it allows us to investigate placement, velocity and acceleration analyses kinematically. The forward dynamics analysis introduces the mass matrix $\mathbf{M}(33 \times 33)$,

and the generalized external force vector $\mathbf{h^a}(33 \times 1)$, as follows:

$$\mathbf{M} = diag(M_1, M_2, \cdots, M_{11}), \tag{4.12}$$

$$\{\mathbf{M}_i = [m_i, m_i, J_i]^T \mid i = 1, 2, \cdots, 11\}, \tag{4.13}$$

$$\mathbf{h^{(a)}} = [h_1^{(a)^T}, h_2^{(a)^T}, \cdots, h_{11}^{(a)^T}]^T, \tag{4.14}$$

$$\{\mathbf{h^{(a)}}_i = [0, -m_i g, 0]^T \mid i = 1, 2, \cdots, 11\}, \tag{4.15}$$

where m_i is the mass of rigid linkage to point i, $J_i = 2l_i/3$ is the polar moment of inertia of rigid linkage to point i, and g is the gravitational acceleration.

4.1.3 Result of the numerical simulation

Table 4.3: Resultant values of kinematic analyses of two mechanisms

Factor	Chebyshev	Theo-Jansen
Step length (SL) [m]	0.454	0.388
Step height (SH) [m]	0.087	0.166
An effective leg length [m]	0.332	0.560
Maximum penetration (δ)	-0.002	-0.008
Capability of the lifting up the leg [%]	26.38	29.620
Step length in trajectory length [m]	94.78	85.340
Average velocity [m/s]	0.099	0.390
Maximum velocity in swing phase [m/s]	1.954	3.052
Minimum velocity in swing phase [m/s]	-0.673	-0.422
Maximum velocity in stance phase [m/s]	0.118	0.043
Minimum velocity in stance phase [m/s]	-0.798	-0.387
Average acceleration [m/s^2]	8.754	9.663
Maximum acceleration in swing phase [m/s^2]	24.312	76.951
Minimum acceleration in swing phase [m/s^2]	6.691	1.892
Maximum acceleration in stance phase [m/s^2]	6.615	48.373
Minimum acceleration in stance phase [m/s^2]	0.104	0.175

At the initial step of the kinematic analysis, each mechanism was examined to be able to draw a closed curve by the end-effector with respect to motions of the input driver to be a rotating-crank with constant angular velocity ω. Generated motions of links are transferred from the driver to the end-effector as the foot link by the kinematic transmission of the system. Further functional aspects of parallel linkages focusing on the the biological nature was investigated by Levin et al. [48] to report an angular relation of geometrical shapes in a continuous mechanical loop called closed kinematic chain (CKC).

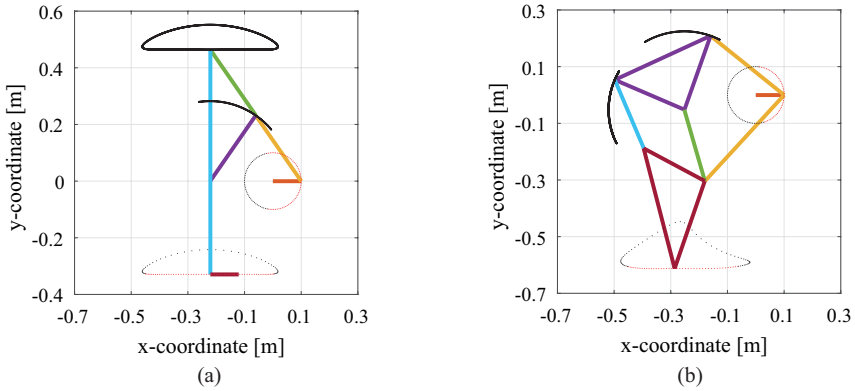

Figure 4-3: Position and posture analyses of two walking mechanisms to generate different locomotive trajectories associated with individual rotations at the input driver. (a) Result in the Chebyshev mechanism and (b) Result in the Theo-Jansen mechanism (b). Individual links colored differently for the discrimination. In each panel, solid black lines and the dotted line represents respectively representative movement trajectories and the leg-motion trajectory of the end-effecter. Red points in the dotted line represents the stance phase.

According to the leg-motion trajectory analysis, the Chebyshev mechanism demonstrated the lowest penetration $\delta = -0.002$ m into the ground, which represents a smooth linear motion with a longer step length in the stance phase SL = 0.454 m that is 94.78% of the total length of step (Figure 4-3(a)). In the Theo-Jansen mechanism, the actual penetration was estimated $\delta = -0.008$ m into the ground, which represents an approximate linear motion in the stance phase with step length SL= 0.3883 m as 85.34% of the total length of step (Figure 4-3(b)), which indicated that the step length is reduced with respect to the ground. The longer steps may introduce a large amount of reaction forces since the contact force depends on the relative deformation. For the sake of simplification to focus on the viscoelastic ground contact, the main body is assumed to kept stationary, which mean that the height of the input driver does not change, and the ground is moving backward at the same velocity as the foot. For the purpose, the speed of the end-effector V_{FV} is focused according to coordinates given by Equation (2.14) with respect to the ground condition. The foot action with respect to the ground is analyzed by the relative velocity

of the end-effector in the form of equation proposed by Shigley [66] as

$$V_{FT} = V_{VT} + V_{FV}, \tag{4.16}$$

where V_{FT}, V_{VT} and V_{FV} denote respectively the velocity of the foot relative to the ground, the velocity of the system relative to the ground and V_{FV} is the velocity of the foot relative to the system. Interestingly, the vector relation of three terms in Equation (4.16) presents all the relative motions in the system. The stance phase as $V_{FT} = 0$ provides

$$V_{FV} = -V_{VT}. \tag{4.17}$$

The relationship of vectors in Equation (4.16) is only valid when a linkage mechanism is having a fixed walking pattern.

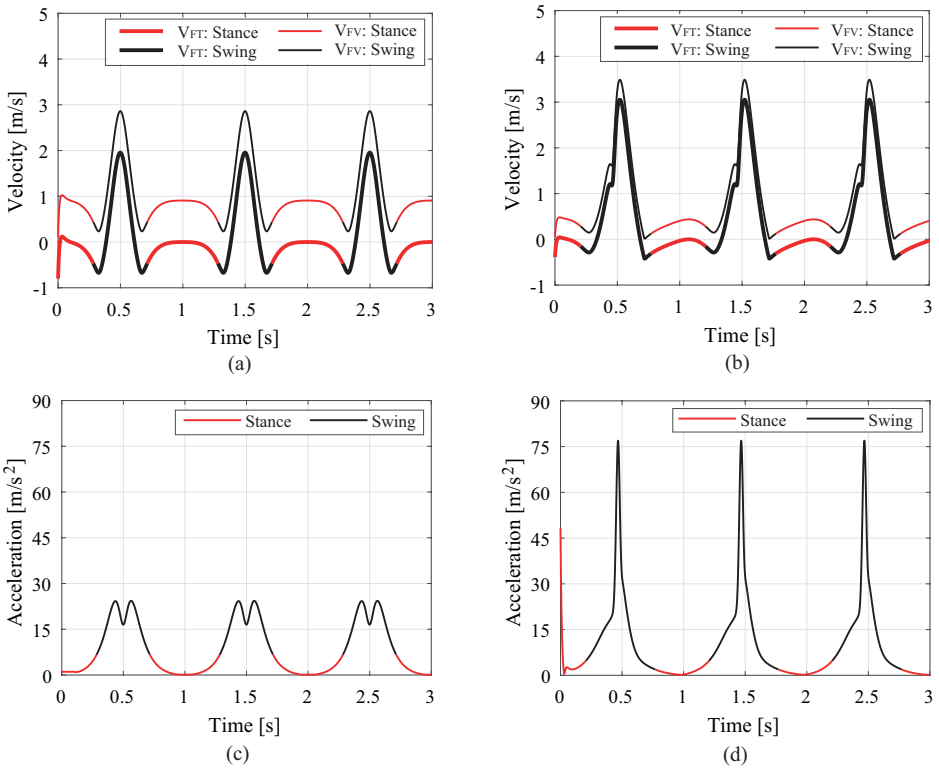

Figure 4-4: Characteristic analyses of the relative velocity VFT and absolute velocity V_{FV} and the acceleration of the foot.(a) and (c) represent respectively velocities and acceleration in the case of the Chebyshev mechanism, and (b) and (d) represent same variables in the case of the Theo-Jansen mechanism. Black and red colors represent respectively swing and stance phases.

In the continuous contact force model, relative contact velocities as dependent features determine whether contacting bodies are approaching or separating [67]. The velocity vector $[\dot{x}, \dot{y}]$ and acceleration vector $[\ddot{x}, \ddot{y}]$ of the potential contact point are obtained from forward dynamic analyses. Thus, the velocity of the end-effector relative to the ground is reconsidered according to the vector in Equation (4.16), and then the velocity was almost zero at the mid-point of the stance phase for two mechanisms, as the desired condition. The condition crucially contributes to the evaluation of dynamic behaviors of the foot-ground interaction since reaction forces are given by explicit functions of state variables. Figure **??** showed absolute values of relative velocities as $\sqrt{\dot{E}_x + \dot{E}_y}$ for the Chebyshev and $\sqrt{\dot{F}_x + \dot{F}_y}$) for Theo-Jansen mechanisms and accelerations as $\sqrt{\ddot{E}_x + \ddot{E}_y})$ and $\sqrt{\ddot{F}_x + \ddot{F}_y})$ in the same way. The numerical simulation started at the mid-point of the stance phase as explained above. According to the velocity analysis, the Chebyshev mechanism had the maximum velocity of 1.95 m/s in the swing phase, and it went down to 0.117 m/s at the mid-point of the stance phase where the relative deformation is reached at the maximum. In the Theo-Jansen mechanism, the maximum velocity was obtained as 3.05 m/s in the swing phase with a faster leg movement rather than that of Chebyshev, and the velocity went down to 0.0426 m/s at the mid-point of the stance phase which is consistent with a dynamic behavior of the foot-ground interaction. Both mechanisms showed an acceleration in the swing phase with respect to the stance phase. The deceleration just before the stance phase contributes a smooth grounding. Other representative values were shown in Table 4.3.

4.2 Kinetic and energy analysis

By using the compliant contact force model, as described in Chapter 3, reaction forces were expressed as continuous functions of penetrations between two bodies. In the viscoelastic contact force model, elastic and damping terms prevent penetration between contacting bodies. Hence, no explicit kinematic constraint is considered, while force reaction terms are utilized.

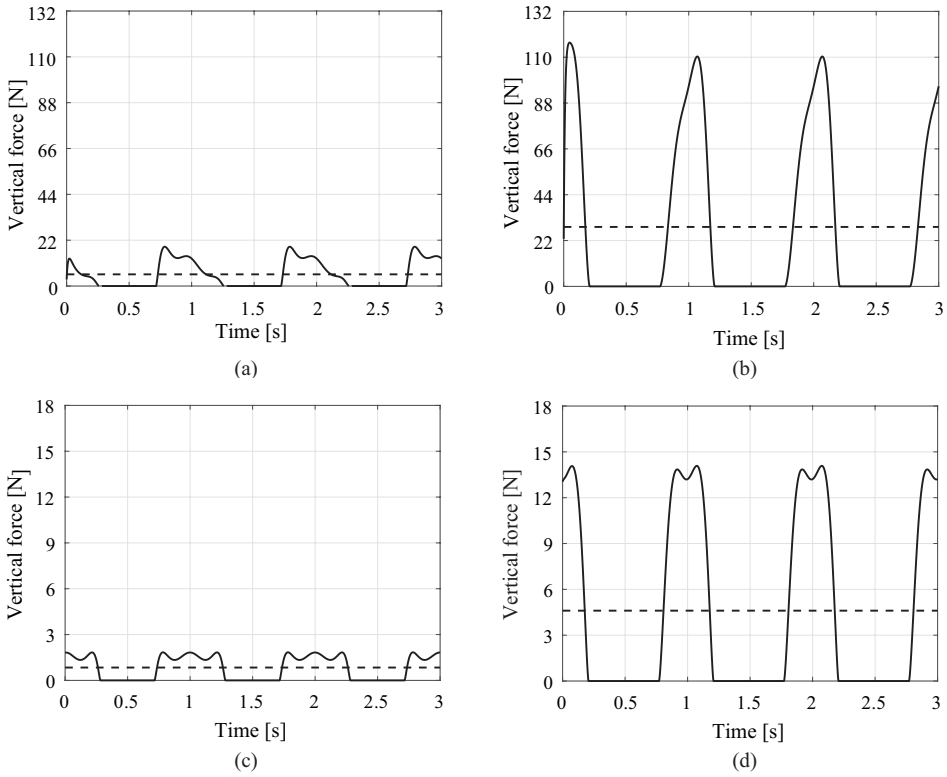

Figure 4-5: Results of contact force analyses in the vertical direction. (a) and (c) represent respectively inelastic and elastic contact conditions in the Chebyshev mechanism, and (b) and (d) represent respectively same variables in the Theo-Jansen mechanism.

In the numerical simulation, the foot-ground vertical reaction force was evaluated by using Lankarani & Nikravesh model [45] with restitution coefficients as $cr = 1.0$ for elastic and $cr = 0$ for inelastic contact conditions. As shown in Figure 4-5, contact forces are zero in the swing phase under the condition that there is no local deformation between the the foot and ground, *i.e.* no contact with the ground. Conversely, the mechanism is in contact with the ground if the force is nonzero. The occurrence of penetration is used for evaluating the local deformation of the contact interaction between foot and ground, which means the stance phase. According to the analysis, the maximum contact force was obtained as 18.859N for the Chebyshev mechanism in the inelastic contact condition and 1.8375N in the elastic case. Average normal force was 5.6079N and 0.8412N respectively. For the Theo-Jansen mechanism, the maximum contact force in vertical direction was 96.0835N for the inelastic contact

condition and 14.0832N in the elastic case. Average normal force was 28.5361N and 4.6052N respectively.

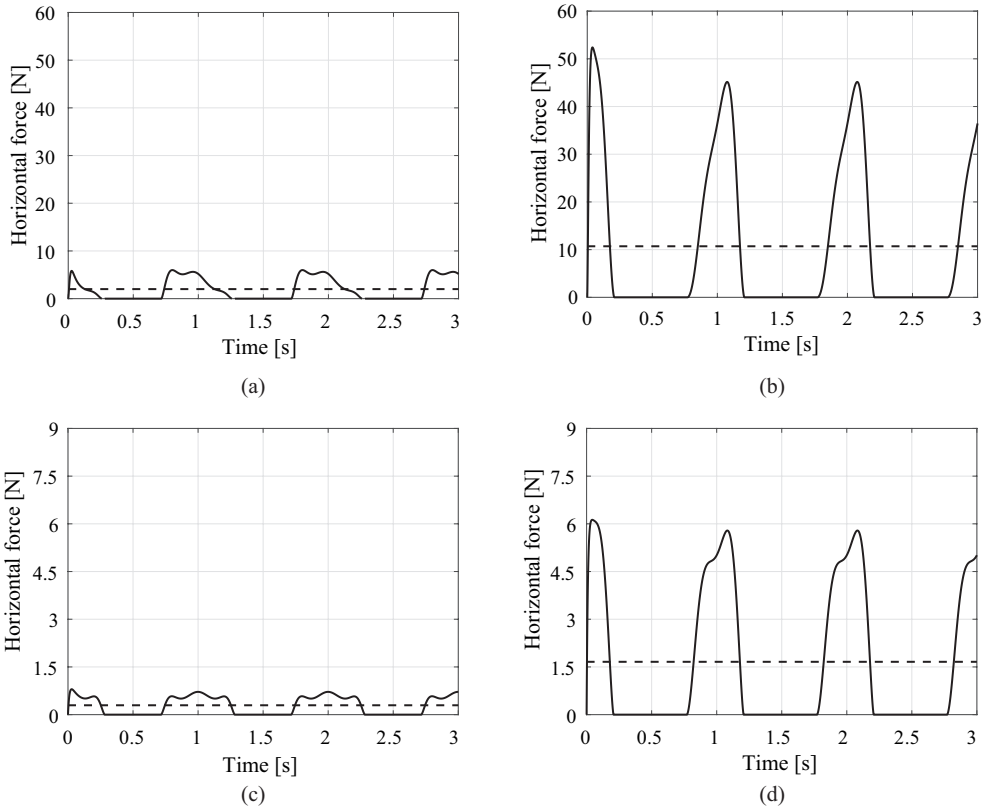

Figure 4-6: Results of contact force analyses in the horizontal direction. (a) and (c) represent respectively inelastic and elastic contact conditions in the Chebyshev mechanism, and (b) and (d) represent respectively same variables in the Theo-Jansen mechanism.

In the consideration of the tangential force acting at the point of contact, the friction and the resultant tangential force f_T due to the deformation at the contact is consistent with the contact force in the horizontal direction as shown in Figure 4-6. In the present study, a specific slipping phenomenon is not covered because of the assumption that the leg is always in contact with the ground in the stance phase. As shown in Figure 4-6(a) and (c), the maximum tangential force was 5.9895N for the Chebyshev mechanism in the inelastic contact condition and 0.7990N in the elastic case (at the mid-point of the stance phase). For the Theo-Jansen mechanism, the maximum friction force was 52.3904N in the inelastic contact condition and 6.1263N in the elastic case, as shown in Figure 4-6(b) and (d).

Torque analyses of two mechanisms were obtained under different contact conditions considering the actual production of resistive load on the input driver.

Table 4.4: Resultant values of dynamic analyses of two mechanisms

Factor [Nm]	Chebyshev	Theo-Jansen
Average absolute driving torque in stance phase during inelastic contact	0.417	0.888
Maximum torque	0.077	5.088
Minimum torque	-0.774	-1.465
Average absolute driving torque in stance phase during elastic contact	0.011	0.018
Maximum torque	0.061	0.714
Minimum torque	-0.154	-0.559
Average absolute driving torque in swing phase	0.083	0.019
Maximum torque	2.280	1.694
Minimum torque	-2.4313	-1.098
Average absolute driving torque during elastic contact	0.056	0.028
Average absolute driving torque during inelastic contact	0.287	0.398

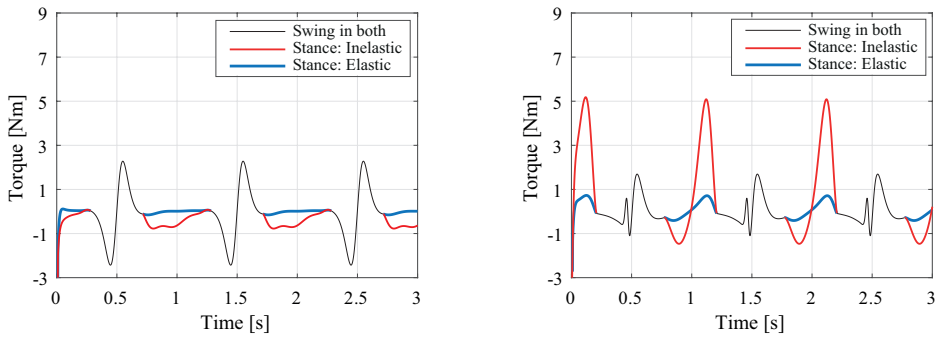

Figure 4-7: Analyses of required driving torques for walking under different contact conditions. (a) Results in the Chebyshev mechanism and (b) results in the Theo-Jansen mechanism.

As shown in Figure 4-7, the negative driving torque was observed in the stance phase for the Chebyshev mechanism because the input driver reversely rotates against the moving direction of the end-effector and therefore the resistive load increases in the phase. It may be associated with "geometrical work" in the report of Waldron and Kinzel [68] that back-driving actuators waste power. The requirement of the geometric work in the Theo-Jansen mechanism in swing and stance phases was comparatively smaller than that of Chebyshev. Other representative values were shown in Table 4.4.

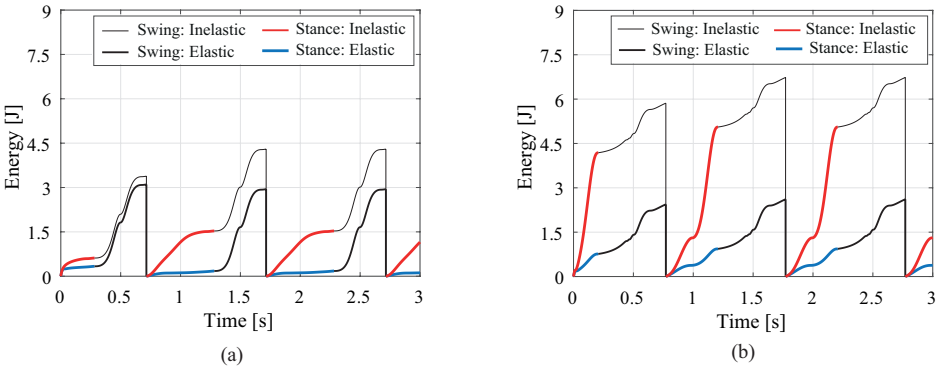

Figure 4-8: Energy consumption of two walking mechanisms in different contact conditions. (a) Results in the the Chebyshev mechanism and (b) results in the Theo-Jansen mechanism.

The energy consumption of two walking mechanisms was calculated during the clockwise (CW) rotation of the input driver, considering the different contact conditions. As shown in Figure 4-8, for the Chebyshev mechanism, the energy consumption in

swing and stance phases was obtained 2.7686 J and 0.1769 J, respectively. In the case of the Theo-Jansen mechanism, the energy consumption in swing and stance phases were 1.6773 J and 0.9362 J, respectively. During the inelastic contact, for the Chebyshev mechanism, the energy consumption in swing and stance phases was obtained 2.766 J and 1.5314 J, respectively. In the Theo-Jansen mechanism, the energy consumption in swing and stance phases were 1.6774 J and 5.0556 J, respectively.

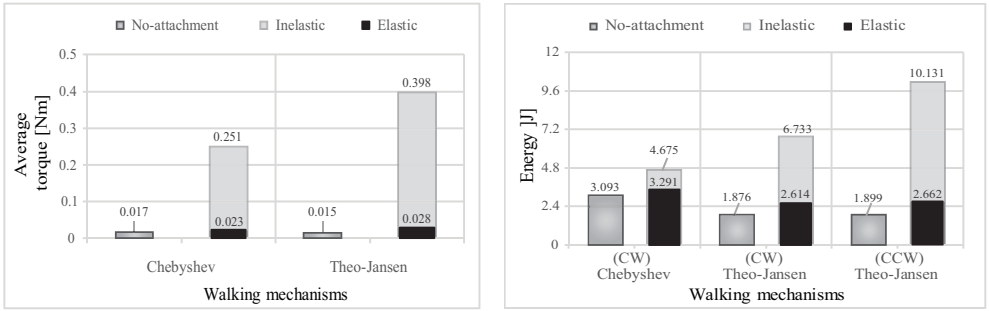

Figure 4-9: Comparative analyses of the average torque (a) and the total energy consumption (b) of two walking mechanisms in different contact conditions. CW and CCW represent respectively conditions of the clockwise input driver rotation and the counter clockwise rotation.

As shown in Figure 4-9, the energy consumption significantly was reduced in the elastic contact conditions commonly in two mechanisms. The tendency is high in the Theo-Jansen case rather than the Chebyshev case. For the validation of the comparative analyses, the same clockwise rotation was given in two walking mechanisms as explained. In the sense of the moving direction, the counter clockwise rotation of the input driver is required to the Theo-Jansen mechanism for going forward. In the comparison of conditions of the clockwise (CW) and the counter clockwise (CCW) rotations of the input driver, the reduced energy consumption was consistently evaluated. The horizontal force or friction was different depending on the moving direction.

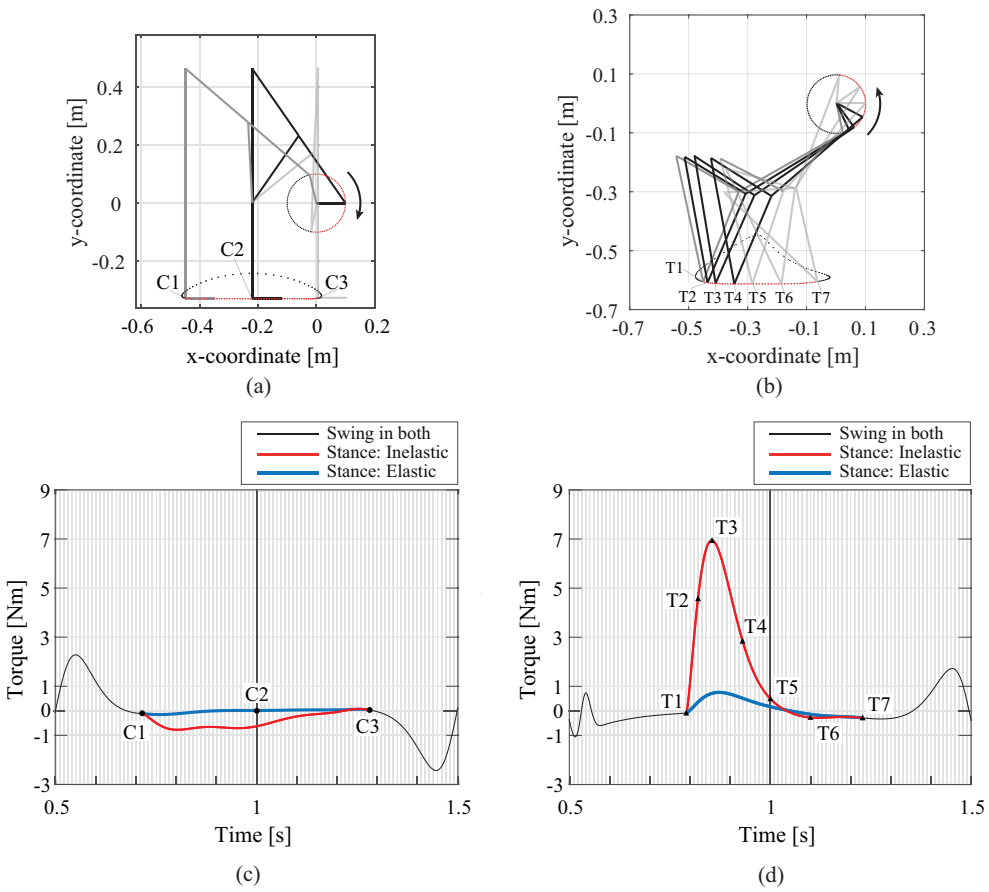

Figure 4-10: A detail analysis on the contact point in each walking mechanism. (a) and (c) represent respectively the position analysis and required driving torque in the single cycle in the case of the Chebyshev mechanism, and (b) and (d) represent same variables in the case of the Theo-Jansen mechanism. In the position analysis of the Theo-Jansen mechanism, links of L_1,L_6,L_9,L_{10} and L_{11} were only displayed as the highlight of the contact phenomenon. Representative time points with labels as C* and T* were selected from the mid-point of the stance phase and changing points of the temporal sequence of each driving torque.

The further analysis on the process when the foot is contacting with the ground was shown in Figure 4-10. The result showed a significant reduction of the required driving torque at the early stage of the stance phase in the case of the Theo-Jansen mechanism as the effect of viscoelastic ground contact.

Chapter 5

Comparison between the proposed method and the other methods

In this chapter, we discuss about the importance of numerical stability in computational methods dealing with multibody system and to show how the stability is achieved in our proposed method in comparison with other existing method. Stability of numerical solution is one of the challenging issue in multibody computer system analysis. Our method is not changing the structure of the general MBD techniques, instead it combines different analysis by introducing a new branches that threat external force in addition to conventional MBD simulation workflow as discussed in Chapter 1 and 3. Traditionally there are two method in analysis of contact impact event in multibody system, namely, discrete and continuous. Either of these two methods is suitable for computational analysis of multibody dynamics. Furthermore implementing any of these methods in forward dynamics analysis as presented in Chapter 2, program requires a special attention to several computational issues related to the accuracy and mathematical representation of contact constraint. Method should be possibly applied into the analysis of various different examples of mechanical system that experience the contact impact. Therefore, to make systematic comparison, particular attention is given to the most popular approaches, that are, Lagrangian formulation, continuous contact force analysis. Finally, two examples of application are considered to compare the accuracy and computational cost of the methods used

throughout this chapter.

5.1 Demonstrative example 1

The first example is the impact of free falling ball on the ground, one of the simplest contact system. Figure 5.1 (a) and (b) shows contact kinematics of system both in Lagrangian approach and penetration model in continous contact force analysis.

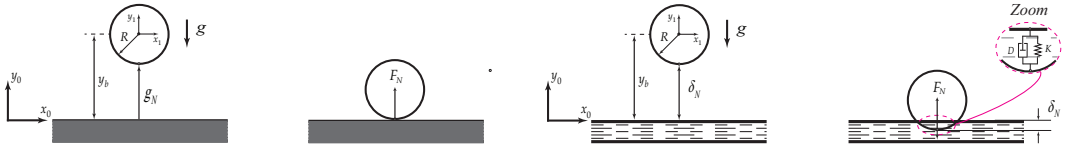

Figure 5-1: Kinematic model of ball-ground contact on Langrangian based approach and penetration model in proposed integrated framework (b).

The ball with mass of 1.0 kg and moment of inertia equal to 0.1 kg m^2, radius of 0.1 m is released from the 1 m initial height under the action of gravitational downward force. Thus, ball falls down until it collides with ground, which is considered to be fully rigid and stationary for the case of contact kinematic model in Figure 5.1 (a). In this example, Lagrangian approach was initially introduced a linear complementarity condition due to impenetrability in impacting objects in order to have unique solution on the contact reaction forces. Therefore condition imposes a gap distance where no penetration is accepted. The same initial configuration was set in the kinematic model with penetration in Figure 5.1 (b) , the ball rebounding is depend on values of input coefficient of restitution.

5.1.1 The linear complementarity problem

Complementarity formulation is based on the fact that in contact dynamics either the relative kinematic variable is zero and the corresponding constraint force is nonzero, or viceversa. In the case of normal contact, if the gap distance is zero, then the normal force is not zero. For two dimensional problems using the complementarity

rule to model the contact yields a linear complementarity problem (LCP) which can be solved using algorithms based on linear programming such as Lemke's algorithm and other.

$$g_N = y_b - R \tag{5.1}$$

which yields,

$$g_N = \begin{cases} g_N > 0 & F_N = 0 \\ g_N = 0 & F_N > 0 \end{cases} \tag{5.2}$$

Equations (5.1) and (5.2) represent an inequality complementarity behavior, for which the product of the relative normal gap and normal contact force is always zero, that is,

$$g_N \geq 0, \quad F_N \geq 0, \quad g_N \cdot F_N = 0 \tag{5.3}$$

Thus, the relation between the gap distance and normal contact force can be subjected to the inequality complementarity condition in its standard form can be written as

$$y = Ax + b, \quad y \geq 0, \quad x \geq 0, \quad y^T x = 0 \tag{5.4}$$

The unknowns in Equation (5.4) are the vector y and x which contains the relative acceleration and contact force.

The equations of motion for the moving ball can be expressed at the velocity level as

$$M_M(u_E - u_A) - h_M \Delta t - W_{NM} f_N = 0 \tag{5.5}$$

where velocity u_E and position u_A are obtained from equation of motion and integrating velocity at instant of time. Those variables in equations of motion can be expressed as

$$M = m \tag{5.6}$$

$$h = -mg \tag{5.7}$$

$$W_N = (1) \tag{5.8}$$

by introducing above mentioned variables, the scalar LCP can be formulated as

$$A = m^{-1} \tag{5.9}$$

$$b = u_A(1 + \varepsilon_N) - g\Delta t \tag{5.10}$$

The set of algebraic equation solved with linear complementarity problem (LCP) formulation by lagrangian approach. By integrating velocity, position at the end of the time step can be calculated as

$$q_E = q_M + \frac{1}{2}\Delta t u_E \tag{5.11}$$

where q_M is the midpoint state variable of Moreau's time-stepping algorithm with an LCP formulation.

$$\ddot{g}_N = AF_N + b \quad \xrightarrow{yields} \quad \ddot{g}_N \geq 0, \quad F_N \geq 0 \quad \ddot{g}_N F_N = 0 \tag{5.12}$$

An LCP can have a unique solution, multiple solutions or no solution at all. All existing solutions can be found using enumerative methods [69], which which are designed to find one unique solution of the LCP. There are multiple solver algorithms available for use but to minimally using it as function to get a solution we described a form of Matlab function with input and output variables.

$$(x, y) = LCP(A, b) \tag{5.13}$$

For large dimensions, enumerative methods become computationally costly because the LCP of dimension n provides $2n$ different combinations of n variables.

5.1.2 Energy analysis

The simplest way to quantify the energy loss during a contact period is based on the energy balance equation proposed by (Beer and Johnston 1997) for the system of two spheres

$$\Delta E = T^{(-)} - T^{(+)} = \frac{1}{2}m_i\left[\left(v_i^{(-)}\right)^2 - \left(v_i^{(+)}\right)^2\right] + \frac{1}{2}m_j\left[\left(v_j^{(-)}\right)^2 - \left(v_j^{(+)}\right)^2\right] \quad (5.14)$$

Considering the kinetic energies before and after impact, the energy loss can be expressed as a function of the coefficient of restitution and impact velocity. Dissipated energy can be estimated with initial impact velocity and given coefficient of the restitution at the instant of time t according to Lankarani & Nikravesh (1990).

$$\Delta E = \frac{1}{2}m_i\left(\dot{\delta}^{(-)}\right)^2\left(1 - c_r^2\right) \quad (5.15)$$

where m is the equivalent mass of the two bodies and c_r is the restitution coefficient in contact force model described in Equation 3.7. In our analysis, m can be found with only mass of the ball since the ground is stationary. Equation provides only dissipated energy at instant of time t. Total energy loss can be evaluated by the integration of contact force around the hysteresis loop of contact force model.

5.1.3 Result and comparison

A computational experiment was conducted to compare above mentioned methods under equivalent condition.

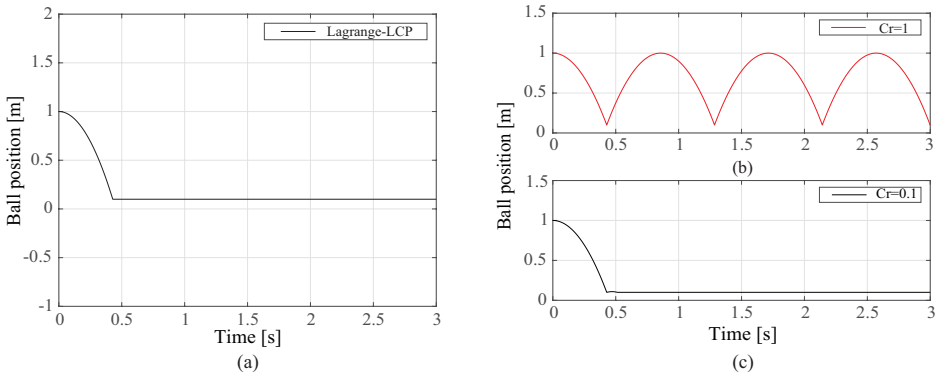

Figure 5-2: Simulation result of kinematic analysis of ball-ground interaction, Ball position (a) Lagrange method and (b),(c) of proposed method during elastic and inelastic contact, respectively.

As shown in position analysis in Figure 5-2, there was no significant differences in position analysis in Lagrange method compared to inelastic condition in proposed method. However, during the elastic contact, rebounding effect of the ball indicated in proposed approach due to the energy interconversion in the system as shown in Figure 5-2 (b).

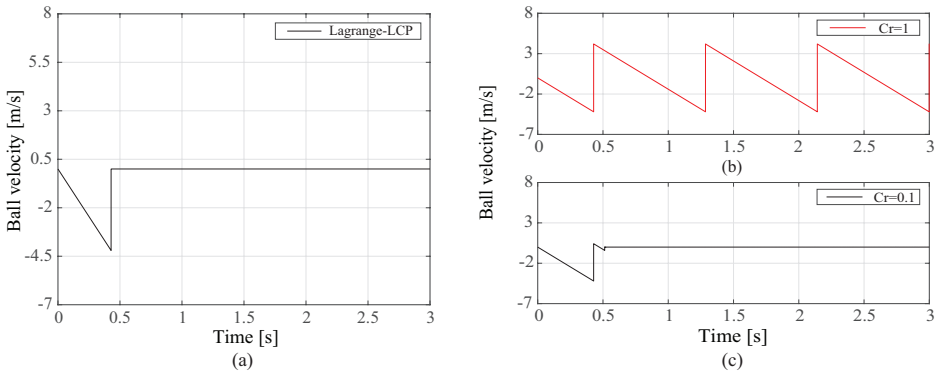

Figure 5-3: The result of velocity analysis

In the velocity analysis, its clearly shown in Figure 5-3 (a) and (c) that velocity drops to the zero just after impact for the case of Lagrangian method as well as with inelastic condition in proposed method after small rebounding. The contact occurs at the same instant time and the ball velocity was consistent with contact-impact dynamics in two methods.

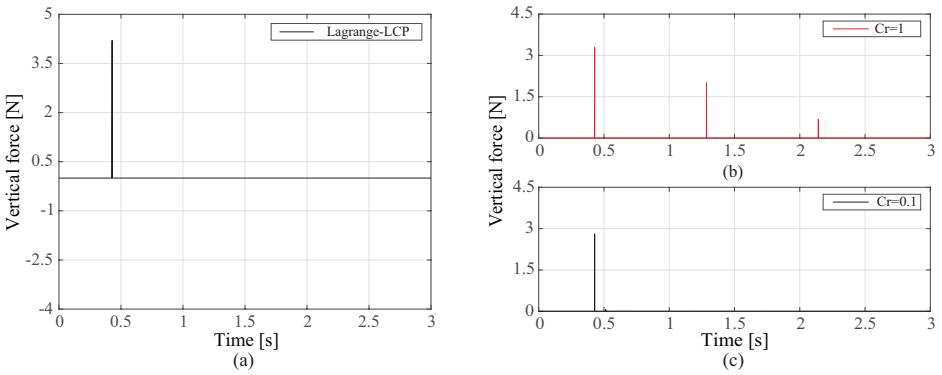

Figure 5-4: The result of contact force analysis

Since the ball is free falling from the predefined height, there is only mass and gravitational downward forces acting on the center. When the initial impact detected contact force estimated for Lagrange method with solver algorithm used to find a unique solution and result of reaction force determined with Lagrange multiplier. In the continuous approach, contact force estimated as a non-linear function of penetration as well as material properties of the ball with constitutive laws proposed by Lankarani & Nikravesh (1990). As shown in Figure 5-4, the contact occurs repeatedly due to the rebounding of the ball. On the other hand, in inelastic contact, ball stays on the ground just after impact without rebounding while time history of force analysis was consistent in two methods.

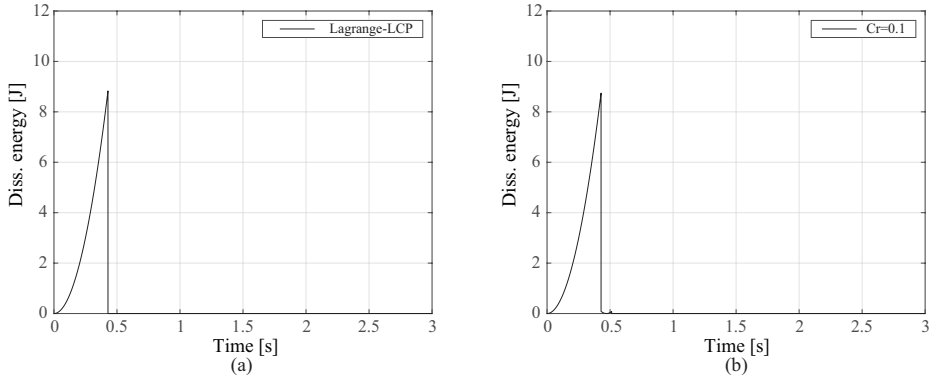

Figure 5-5: Energy dissipation during an contact

Dissipated energy due to the internal damping is shown in Figure 5-5. There was no significance difference found in two methods for the case of inelastic contact.

Interestingly, force-penetration diagram shows that there was no energy dissipated during the elastic impact with ground.

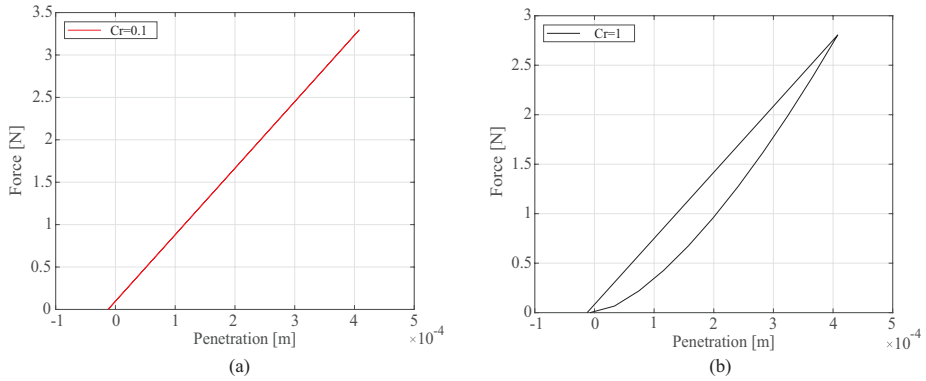

Figure 5-6: Force penetration relation in proposed method during elastic contact (a) and inelastic contact (b).

A computation time during the simulation was measured with Matlab function *cputime* returns the total CPU time (in seconds) used by each method from the time it was started.

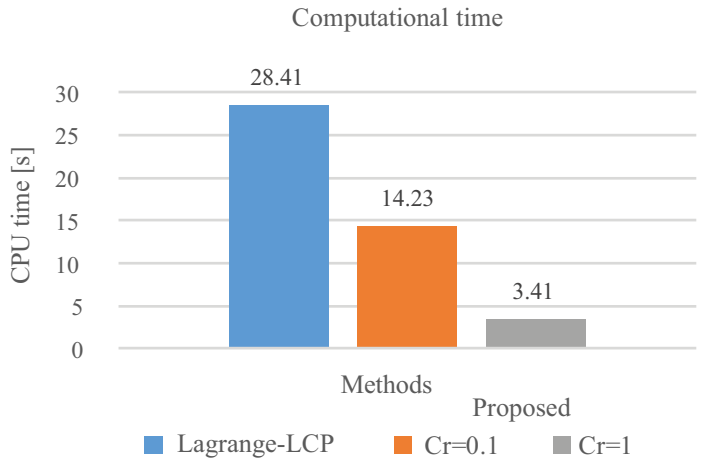

Figure 5-7: Result of total computation time in numerical experiment in two methods.

The total simulation time was comparatively higher in Lagrange method as shown in Figure 5-7 because the ball remains on the ground after impact and algorithm further processing to find a unique solution by recalling a solver function. On the other

hand, proposed method uses twice smaller processing time even in same condition as inelastic contact occurs. Applicability of the Lagrange method is taken granted if contact dynamics of system is a clear, for instance its used in treatment of contact force analysis in rail-road dynamics where bodies are always in contact or formulated with strict constraint. However, based on the comparative analysis, proposed methods has shown advantages compared to Lagrangian method even in simple example of free falling ball.

5.2 Demonstrative example 2

A simple example of ball-ground contact clearly demonstrated the use of Lagrangian method for open-loop system with unilateral contact as well as penetration model as integration into proposed method. Since there is no constraint imposed condition accuracy becomes a not critical issue. We proposed a new experimental setup with slider crank mechanism subject to contact impact with another free block which has certain application to compliant force generator mechanism [70].

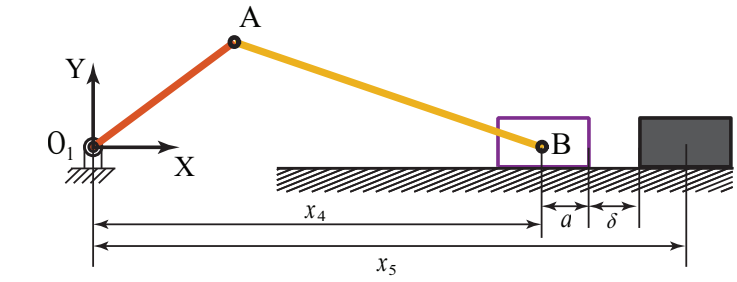

(a)

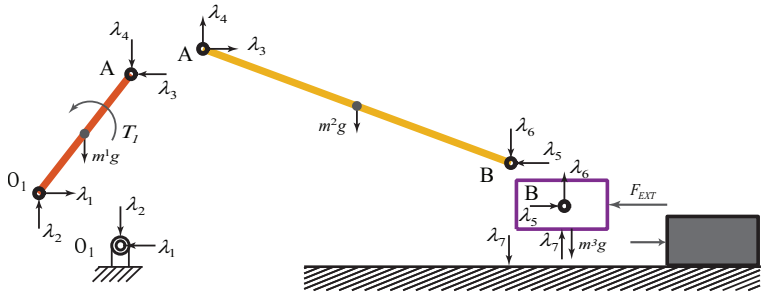

(b)

Figure 5-8: Kinematic model for slider-crank mechanism (a), Corresponding free body diagram of constrained mechanical system.

In the assumption that the multibody system consists of constrained bodies and constraints according to the interaction with the ground, equations of motion must contain reaction forces corresponding to free body diagram (FBD) to analyze the dynamics of a system. The reaction forces are included in equations of motion based on FBD of a system as shown in Figure 5-8 (b). Slider-crank mechanism in Figure 5-8 (a) is constrained, therefore, reaction force appears at the joints which can be expressed with Lagrangian multipliers, the result of DAE of motion. The external force F_{EXT} acting on the constrained system when it impact the object has opposite direction and applied on the joint B of slider unit.

5.2.1 Formulation with Lagrangian approach

There are two main approaches that can be used in multibody system formulations to obtain the contact force when slider impact with the another free block. In the first approach, the contact between slider block and free block is described by kinematic

constraint equation. The contact force can be obtained as the reaction force due to the imposition of the contact constraints with Lagrange multipliers [71]. When equality constraint are used, it is assumed that there is no penetration or separation between the contact constraints which is

$$\Phi\left(q, s, t\right) = 0 \tag{5.16}$$

where q is the vector of system generalized coordinates, s is the vector of the surface parameter, and t is the time. As discussed in Chapter 2, after differentiating the preceding equation twice respect to the time, the constraint equations at the acceleration level can be written as

$$\mathbf{\Phi}_q \ddot{\mathbf{q}} + \Phi_s \ddot{s} = \gamma \tag{5.17}$$

Φ_q and Φ_s are the sub-Jacobians of the constraint equation associated, respectively, with the generalized coordinates q and surface parameters s; and γ is the quadratic velocity vector.

$$\begin{bmatrix} M & 0 & \Phi_q^T \\ 0 & 0 & \Phi_s^T \\ \Phi_q & \Phi_s & 0 \end{bmatrix} \begin{Bmatrix} \ddot{q} \\ \ddot{s} \\ \lambda \end{Bmatrix} = \begin{bmatrix} h^{(a)} \\ 0 \\ \gamma \end{bmatrix} \tag{5.18}$$

These equation can be solved to determine the acceleration $\ddot{q}$ and $\ddot{s}$ as well as vector of Lagrange multipliers λ. In the constraint contact formulation, the constraint equation must be satisfied at position, velocity, and acceleration level without violation. However, above mentioned formulation, Baumgarte's stabilization techniques no longer applicable in acceleration equation. Therefore, formulation on acceleration level including the contact constrained is considered to be index 1 system. In order to reduce the constraint violation and maintain the stability of equation of motion in position and velocity level, index 2 formulation can be introduced as

$$q(0) = q_0, \tag{5.19}$$

$$v(0) = v_0, \tag{5.20}$$

$$\dot{q} = v, \tag{5.21}$$

$$M\dot{v} = h^{(a)} + W^T\lambda, \tag{5.22}$$

$$M\left(v_j^+ - v_j^-\right) = W_j^T\Lambda_j, \tag{5.23}$$

$$0 \leq g \perp \lambda \geq 0, \tag{5.24}$$

Starting from the initial conditions (5.16)-(5.17), the system's state given by position q and velocity v are described by a non-impulsive behavior. It is influenced by the generalized mass matrix M and right hand side forces $h^{(a)}$. Due to the Signorini-Moreau condition (5.21), gap distance g_N affect this type of motion by varying contact force parameters λ. The notation $g \perp \lambda$ stands for $g^T\lambda = 0$. The force parameters weight the columns of W^T in the equations of motion (5.19). For countable time instances t, the velocities jump enforced by an impact Λ_j according to (5.19). With (5.18), the position q can be calculated by the fundamental theorem of calculus for differentiable functions. One might think that the complementarity problem (5.16)-(5.21) is integrated best by an event-driven time-integration strategy. However as event-driven schemes resolve the exact time of impact, they cannot accurate enough.

$$g_N = x_5 - x_4 - a \quad \xrightarrow{yields} x_5 - L_1\cos\theta_1 + L_2\cos\theta_2 + a\cos\theta_3 \tag{5.25}$$

$$M = \begin{pmatrix} J_1 + l_1^2\left(\frac{m_1}{4} + m_2 + m_3\right) & l_1 l_2\cos\left(\theta_1 - \theta_2\right)\left(\frac{m_2}{2} + m_3\right) \\ l_1 l_2\cos\left(\theta_1 - \theta_2\right)\left(\frac{m_2}{2} + m_3\right) & J_2 + l_2^2\left(\frac{m_2}{4} + m_3\right) \end{pmatrix} \tag{5.26}$$

$$h^{(a)} = \begin{pmatrix} -l_1 l_2 \left(\theta_1 - \theta_2\right) \left(\frac{m_2}{2} + m_3\right) \omega_2^2 - g l_1 \cos\theta_1 \left(\frac{m_1}{2} + m_2 + m_3\right) \\ l_1 l_2 \left(\theta_1 - \theta_2\right) \left(\frac{m_2}{2} + m_3\right) \omega_1^2 - g l_2 \cos\theta_2 \left(\frac{m_2}{2} + m_3\right) \end{pmatrix} \tag{5.27}$$

The bilateral constraint holds slider at fixed y position as

$$g = l_1 \sin\theta_1 + l_2 \sin\theta_2 = 0 \tag{5.28}$$

Linear complementarity problems are the result of other method which mathematically give the exact solution to contact problem where constraint inequality is arises. In the second approach, a compliant contact force with assumed that stiffness and damping coefficient is used to describe the contact-impact phenomenon and its possible to consider the separation [72]. The second approach is integrated in our proposed computational framework. Therefore, proposed method benefits from both constraint formulation and contact force model which will be shown with computational accuracy analysis in this chapter.

5.2.2 Result and comparison

In contact force analysis, force appears at the exact time when slider impact the object was obtained in plot with proposed method. Due to the constraint enforced condition, the timing of contact was different in Lagrangian method. Furthermore, we estimated the simulation error in position and velocity level for the two methods. Representative values are shown in Table 5.1.

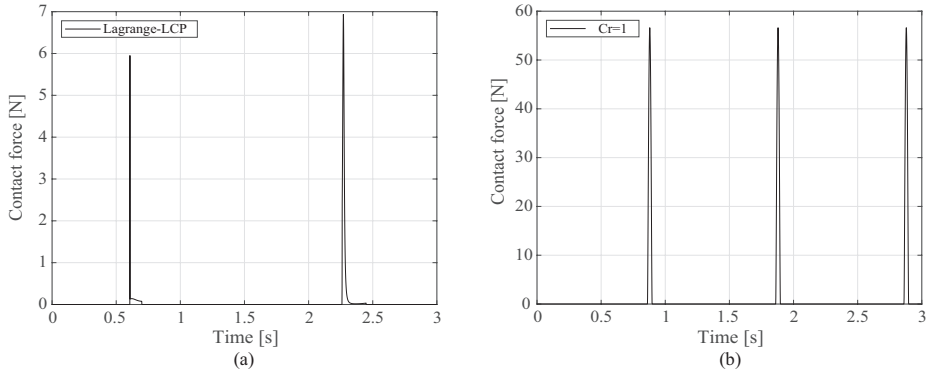

Figure 5-9: Contact force for Lagrangian method (a) and proposed method for inelastic contact (b).

Table 5.1: Resultant values of constraint violation at position level

Factors	Lagrangian approach	Proposed method
Mean error at position constraint	0.0045	7.123
Total accumulated error	1.5585	0.2138

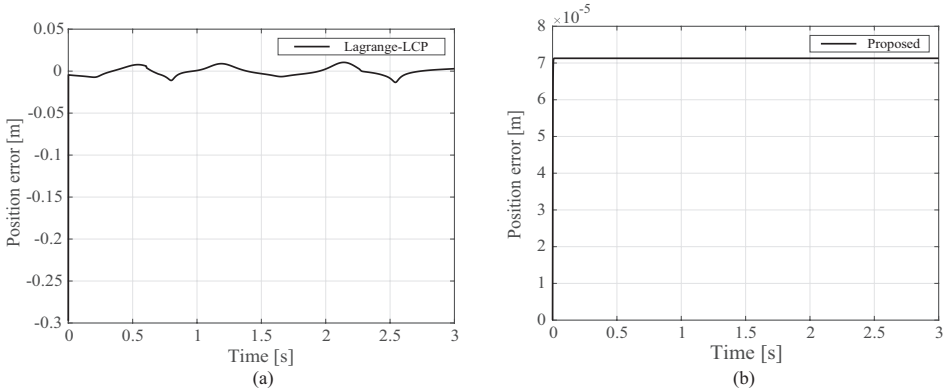

Figure 5-10: Constraint violation at the position level, Lagrangian approach (a) and Proposed method with Baumgarte's stabilization technique (b).

In general, error must be zero or must be enough to give a right answer. In position level, the values are fluctuated due to the constraint imposed condition in Lagrangian approach.

Table 5.2: Resultant values of computation time and force analysis

	Lagrangian approach	Proposed integrated method (Lankarani and Nikravesh)	
Coeff. Rest.	-	$cr = 0.1$	$cr = 1$
Δt [s]	0.429	0.429	1.286
F_{Nmax} [N]	4.204	2.806	3.295
CPU time [s]	28.4063	14.2344	3.4063

Baumgarte's stabilization technique initially implemented in conventional MBD approach which makes proposed framework to be general and simple. The mean error was kept in values as shown in the table just after a few millisecond when the system reached at stable state. Total accumulated error was comparatively smaller in proposed method. Representative values are shown in Table 5.2.

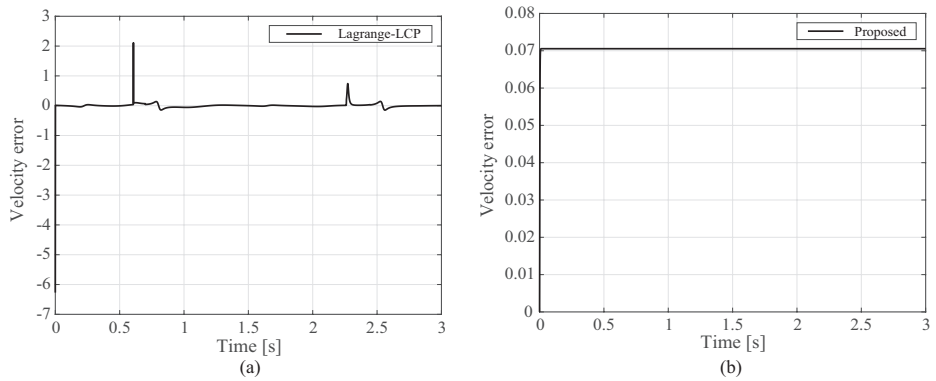

Figure 5-11: Constraint violation at the velocity level, Lagrangian approach (a) and Proposed method with Baumgarte's stabilization technique (b).

Contact relative velocities in constraint was estimated and rebounding of impact velocity was indicated in Lagrangian method. The rebound impact velocity represents the initial instant of impact. When there is no stabilization algorithm that gives accurate solution in velocity before and after impact, at least correct the error at instant time, apparently there is sudden increase of numerical error which may cause the simulation will be no longer proceed. Mean error in velocity level was the same

but total accumulated error was slightly increased in Langrangian method because its the sum of error it each joint that enforced by the impact. Proposed method with Baumgarte stabilization techniques demonstrated the accurate analysis in both position and velocity level. Representative values are shown in Table 5.3.

Table 5.3: Resultant values of constraint violation at velocity level

Factors	Lagrangian approach	Proposed method
Mean error at velocity constraint	0.0705	0.0012
Total accumulated error	211.5316	3.4806

Chapter 6

Dynamic modelling of the horse locomotion

Legged locomotion has been widely studied and tried to rebuild by simple mechanical systems called biological walkers, which were based on open and closed chain mechanical systems [73, 74, 75, 76]. Biological walkers are not only focusing on a benefit of multiplicity of legs [74, 76] but also are highlighted in a less-energy consumption according to the generation of smooth leg trajectories, which is demonstrated by Theo Jansen [65] and confirmed in previous chapter of these thesis. The author of Komoda & Wagatsuma [7] demonstrated that the Theo Jansen mechanism walks with less energy consumption with respect to hexapods [74, 76] when it is moving with a slow walking speed, while it is getting worse in the high-speed walking. However, it is known that the animal locomotion changes depending on the speed of mobility, especially in horses, which exhibit gait pattern transitions [77, 78, 79, 80] presumably for minimization of the energy consumption. In the consideration of analyses on the energy efficacy of the animal locomotion with a high-speed mobility, the kinematic model based on a simple mechanism such as closed linkages has advantages yet it requires the mechanism with a high duty-factor [79, 81] which is defined as the fraction of the duration of a stride for which each foot remains on the ground, or the ratio between stance and swing phase. Interestingly, possible extensions of closed linkage mechanism were reported [82, 49, 83] in order to change the duty-factor.

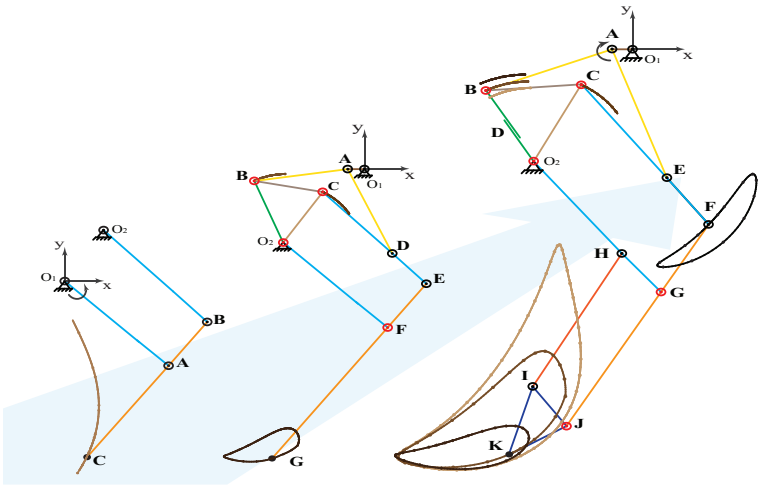

Figure 6-1: Implementation of horse leg mechanism. Horse leg mechanism consists of three parts: Reciprocal mechanism, which observed in horse hind limb produces lifting up motion in lower part of the leg. Theo-Jansen like simplified mechanism with cyclic driving unit as shown in the middle. Horse like Leg mechanism with different modifiable footpath, linear actuator inserted and hoof mechanism added based on anatomy of the horse leg.

Coros et. al. [84] propsed the theoretical framework to provide a desired cyclic trajectory based on multiple gears with different diameters and rotation phases connected with linkages by using a solver of the constraint optimization problem and then verified to provide animal leg motions. Their approach has an advantage of the design any free form of cyclic motion can be generated by the combination of multi-gears with a simple linkage as the kinematic analysis; however their theoretical analysis cannot apply to computation of the force and torque estimation of the mechanism as the kinetical analysis as presented in Chapter 2 of this thesis. In the sake of kinematic and kinetical analysis of the horse leg motion as the representative animal with a high-speed mobility, we hypothesized that the musculoskeletal system can be modeled based on closed linkages as shown in Figure 6-1 and found a critical link to effectively control the shape of leg trajectories. Once the functional relationship of muscle-tendon units can be represented by the simple closed-linkage system, the model allow us to investigate how the leg trajectory is modifiable in the displacement analysis in the kinematic analysis and when and where the leg has the maximum torque in the inverse kinematic analysis. This method will reveal what

kinematic transmission are derived from the input to the end-effector as toe by applying changes of parameters to represent leg components.

6.1 Biomechanics of horse locomotion

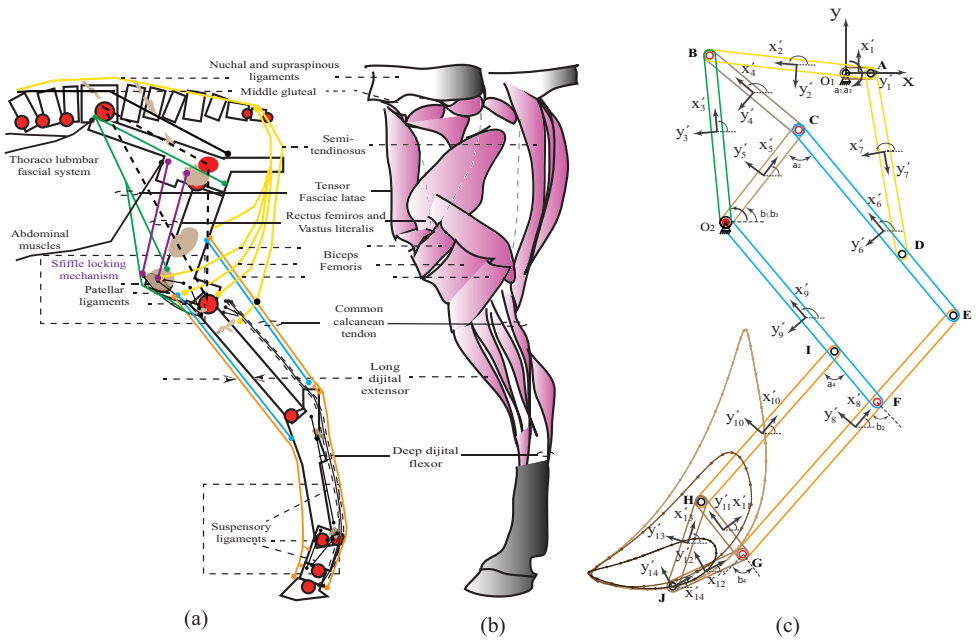

Figure 6-2: Schematic illustration of the musculoskeletal system of the horse hind limb (a) Associations of bones and joint positions, (b) the muscle organization and (c) the proposed model with closed linkages. Figures (a) an (b) were drawn based on analyses of Budras et al. (2012) [1].

In the horse body, reciprocal mechanism in hind limb, basics of functional anatomy observed in vitro experiment [85], confirmed by vivo measurement [86] are shown in Figure 6-2 (a), (c) with blue and orange lines to represent the stifle and the hock move individually. The mechanism produces a lifting-up trajectory that allows the horse to navigate the lower limb in a smooth and coordinated manner as shown in Figure 6-3 (c). Mechanics of the horse leg was explained by Hoyt et. al. [78] and Hildebrand [87] with its anatomical point of view. A purely qualitative investigation of rear-leg external anatomy shows a similarity in this proposed design in shape and size of the distal region, while that the proximal limb (rump) is larger and more rounded than the equivalent shoulder region indeed. Figure 6-3 (a) and (b) provided the musculoskeletal

structure of whole hind limb which we focused on. The red circles represent joints in horse limb correspond to the B, C, O_2, F, G joints in proposed leg mechanism except the joints placed in suspensory part. Musculoskeletal structure of hind limb was represented by simple shapes such as triangle in upper limb dotted by big red circles in Figure 6-3 (a), which is controlled by tensor fascia muscles and series parallelogram in lower limb represented by blue and orange colors known as reciprocal apparatus. The triangle structure in the toe which contacts with the ground known as hoof formed by links drawn by orange lines except to the suspensory ligaments. Thus, all of these connections provides the unique structure of walking in the viewpoint of closed linkages. It leads an operating principle of the horse leg mechanism to have an upper and lower 3-bar mechanism forms a rigid triangle that allows parallelogram linkage to change the shape and guide motion of one another. Finally, motion transferred from second parallelogram to the hoof part. Same principle operates in the Theo-Jansen mechanism [82, 83, 84] in case of simplified model illustrated in Figure 6-1 (b). However, none of related past related works [14-16] have not yet reported the importance of an additional linear translational actuator, which is critically control the shape of the leg trajectory. We focused on the original perspective and applied this principle to reciprocal apparatus and the hoof part in proposed leg mechanism in Figure 6-3(c). In the following section, the function was evaluated with multibody dynamics.

6.2 Kinematic analysis of horse leg mechanism

In this Chapter, we introduced a closed-linkage mechanism inspired from muscleskeletal structure of horse hind limb, regenerate horse-like flexible leg trajectories.

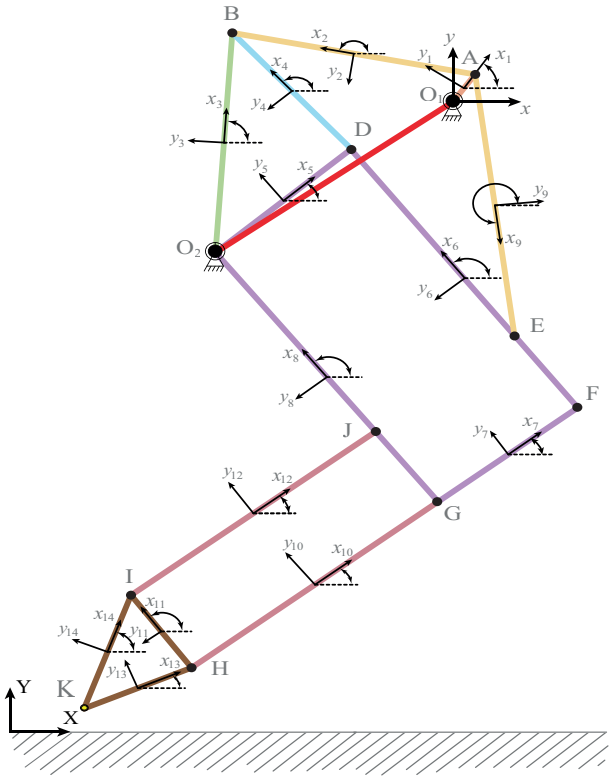

Figure 6-3: Kinematic model of the horse leg mechanism, generalized coordinates in constrained segments were placed on the center of each link.

The kinematic model for the horse leg mechanism is illustrated in Figure 6-3, the vector q with 42 elements including position and orientation of each body in leg mechanism expressed as generalized coordinates as follows:

$$\mathbf{q} = [q_1^T, q_2^T, q_3^T, q_4^T, q_5^T, q_6^T, q_7^T, q_8^T, q_9^T, q_{10}^T, q_{11}^T, q_{12}^T, q_{13}^T, q_{14}^T]^T \tag{6.1}$$

The vector of q contains 42 ($= 14 \times 3$) elements which are 6 rigid links and their center of position x_i, y_i and orientation ϕ_i are obtained in the generalized coordinates in the present analysis. A set of kinematic algebraic constraint equation according to the initial configuration for the position analysis can be written

$$\mathbf{\Phi}(\mathbf{q},t)=\begin{bmatrix}\Phi^K(q)\\ \Phi^D(q,t)\end{bmatrix}=\begin{bmatrix}
x_1-L_1\cos\theta_1\\
y_1-L_1\sin\theta_1\\
x_2-L_2\cos\theta_2-x_1-L_1\cos\theta_1\\
y_2-L_2\sin\theta_2-y_1-L_1\sin\theta_1\\
x_3+L_3\cos\theta_3-x_2-L_2\cos\theta_2\\
y_3+L_3\sin\theta_3-y_2-L_2\sin\theta_2\\
x_3-L_3\cos\theta_3-a_x\\
y_3-L_3\sin\theta_3-a_y\\
x_4+L_4\cos\theta_4-x_2-L_2\cos\theta_2\\
y_4+L_4\sin\theta_4-y_2-L_2\sin\theta_2\\
x_5+L_5\cos\theta_5-x_4+L_4\cos\theta_4\\
y_5+L_5\sin\theta_5-y_4+L_4\sin\theta_4\\
x_5-L_5\cos\theta_5-a_x\\
y_5-L_5\sin\theta_5-a_y\\
x_6+L_6\cos\theta_6-x_4+L_4\cos\theta_4\\
y_6+L_6\sin\theta_6-y_4+L_4\sin\theta_4\\
x_7+L_7\cos\theta_7-x_6+L_6\cos\theta_6\\
y_7+L_7\sin\theta_7-y_6+L_6\sin\theta_6\\
x_8-L_8\cos\theta_8-x_7+L_7\cos\theta_7\\
y_8-L_8\sin\theta_8-y_7+L_7\sin\theta_7\\
x_8-L_8\cos\theta_8-a_x\\
y_8-L_8\sin\theta_8-a_y\\
x_9+L_9\cos\theta_9+L_{61}\cos\theta_6-2L_5\cos\theta_5-a_x\\
y_9+L_9\sin\theta_9+L_{61}\sin\theta_6-2L_5\sin\theta_5-a_y\\
x_9-L_9\cos\theta_9-x_1-L_1\cos\theta_1\\
y_9-L_9\sin\theta_9-y_1-L_1\sin\theta_1\\
x_{10}+L_{91}\cos\theta_{10}-x_7+L_7\cos\theta_7\\
y_{10}+L_{91}\sin\theta_{10}-y_7+L_7\sin\theta_7\\
\theta_{10}-\theta_7\\
x_{11}-L_{11}\cos\theta_{11}-x_{10}+L_{91}\cos\theta_{10}\\
y_{11}-L_{11}\sin\theta_{11}-y_{10}+L_{91}\sin\theta_{10}\\
x_{12}-L_{10}\cos\theta_{12}-x_{11}-L_{11}\cos\theta_{11}\\
y_{12}-L_{10}\sin\theta_{12}-y_{11}-L_{11}\sin\theta_{11}\\
x_{12}+L_{10}\cos\theta_{12}+2L_{81}\cos\theta_8-a_x\\
y_{12}+L_{10}\sin\theta_{12}+2L_{81}\sin\theta_8-a_y\\
x_{13}+L_{12}\cos\theta_{13}-x_{10}+L_{91}\cos\theta_{10}\\
y_{13}+L_{12}\sin\theta_{13}-y_{10}+L_{91}\sin\theta_{10}\\
x_{14}-L_{13}\cos\theta_{13}-x_{13}+L_{12}\cos\theta_{13}\\
y_{14}-L_{13}\sin\theta_{13}-y_{13}+L_{12}\sin\theta_{13}\\
x_{14}-L_{13}\cos\theta_{13}-x_{12}+L_{10}\cos\theta_{12}\\
y_{14}-L_{13}\sin\theta_{13}-y_{12}+L_{10}\sin\theta_{12}\\
\theta_1+\omega t
\end{bmatrix}_{42\times1}=\mathbf{0} \tag{6.2}$$

where the first 41 elements of the column matrix $\Phi^K(q)$ are derived from Equation (2.5) for absolute constraints between body and ground, and Equation (2.4) for constraint equation for revolute joins connecting the rigid links. The last element $\Phi^D(q,t)$ is derived by the driving constraint Equation (2.6).

The partial derivative of position constraint equation respect to the generalized

absolute cartesian coordinates q is Jacobian matrix $\mathbf{\Phi}_q$ is obtained as:

$$\mathbf{\Phi}_q = \left[\frac{\partial \mathbf{\Phi}(\mathbf{q},t)}{\partial \mathbf{q}}\right]_{42\times 42}, \tag{6.3}$$

where it allows us to investigate placement, velocity and acceleration analyses kinematically. The forward dynamics analysis introduces the mass matrix $\mathbf{M}(42 \times 42)$, and the generalized external force vector $\mathbf{h^a}(42 \times 1)$, as follows:

$$\mathbf{M} = diag(M_1, M_2, \cdots, M_{14}), \tag{6.4}$$

$$\{\mathbf{M}_i = [m_i, m_i, J_i]^T \mid i = 1, 2, \cdots, 14\}, \tag{6.5}$$

$$\mathbf{h^{(a)}} = [h_1^{(a)^T}, h_2^{(a)^T}, \cdots, h_{14}^{(a)^T}]^T, \tag{6.6}$$

$$\{\mathbf{h^{(a)}}_i = [0, -m_i g, 0]^T \mid i = 1, 2, \cdots, 14\}, \tag{6.7}$$

where m_i is the mass of rigid linkage to point i, $J_i = 2l_i/3$ is the polar moment of inertia of rigid linkage to point i, and g is the gravitational acceleration.

6.2.1 Classfication of engineering and biological linkages in horse leg mechanism

Except for the engineering classification of the planar linkages driven by cyclic motion as known as Grashof condition, Muller (1996) [88] proposed the analytical classification method focusing on evolutionary changes in the mechanical behavior of the biological linkages. Its linear and non-linear transmission property indicated in living organisms with different parameter such as length and absolute angle. According to the classification, the reciprocal mechanism in horse hind limb based on its anatomical name of the bars coded in type of $2Plsls$ parallelogram linkage. Here number indicates the motion variables and linkage is non-crossed parallelogram based on their length of the bars $a \cong c$ and $b \cong d$, where a, c are the length of long side as noted O_2 to F and E to C as shown in Figure 6-2 (c). The configuration gives a linear transmission of α_2 to β_2 (α-input angle, β-output angle).

Table **??** shows the experimental result of classification for all linkages entered in proposed leg mechanism. Firstly, linear transmission observed in biological linkage. The range of the motion variables α_2, β_2 of $2Plsls$ linkage indicated $[35° - 141°]$, which was close to its working range of biological linkage as previously mentioned. Secondly, Non-linear transmission depending on length of linear actuator L_3 was observed in engineering linkages. Kinematic transmission of the crank-rocker mechanism measured by input angle α_1 output angle β_1 as shown in Figure 6-4. As a result, the amplitude of angular oscillation in rocker link changes depending on length of L_3 link. In addition, amplitude measured on three different values of L_3 link, black triangle correspond to the highest points of the oscillation and red dot represent the lowest points. All links in this leg mechanism formed by one another. Therefore, the relative angle between them describes the amplification of force and speed and acceleration of end effector.

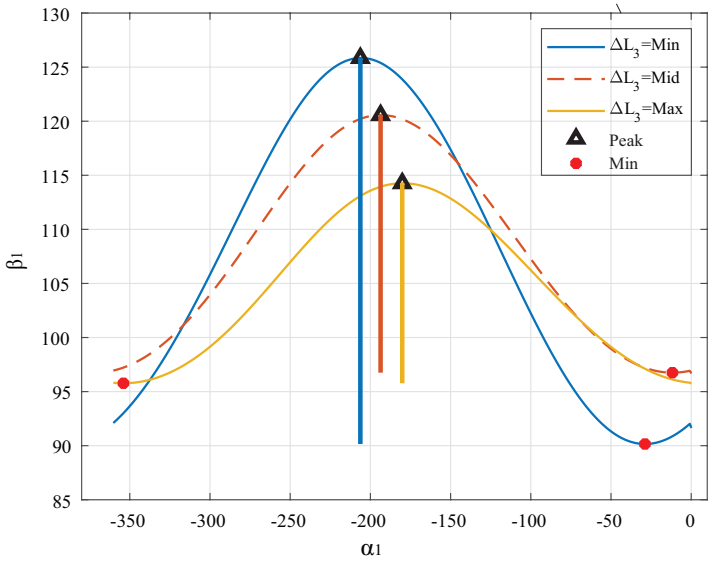

Figure 6-4: An effect of length changes of the L_3 link inserted in horse leg mechanism as important function of muscle-tendon unit

A positive transmission α, β either increases or decreases of the type $2Plsls$, absolute transmission stability obtained in biological system. Working range of output motion variable indicated $[30°-145°]$ in case of the biological linkage driven by muscles in horse hind limb [85]. Before making the classification of mechanism into biological

and engineering linkages, we tested the effect of length changes of L_3 link. Besides, L_3 is the linear actuator connecting B and O_2 grounded node as shown in Figure 6-2 (c), $x_3^{'}$ and $y_3^{'}$ are coordinates located in the center of the body correspond to the absolute coordWinates defining orientation of the body.

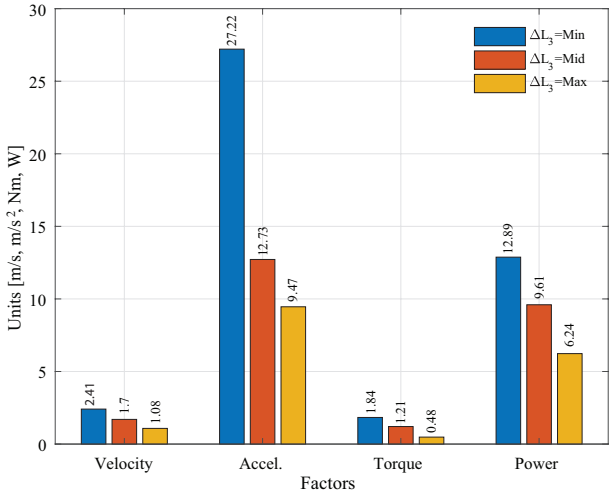

Figure 6-5: Characteristic analysis including end effectors placements in the case of $\Delta L_3 = ave$ (average). (a) the planner trajectory is shown in, (b) velocity analysis, (c) acceleration, (d) and driving torque τ of the proposed leg mechanism.

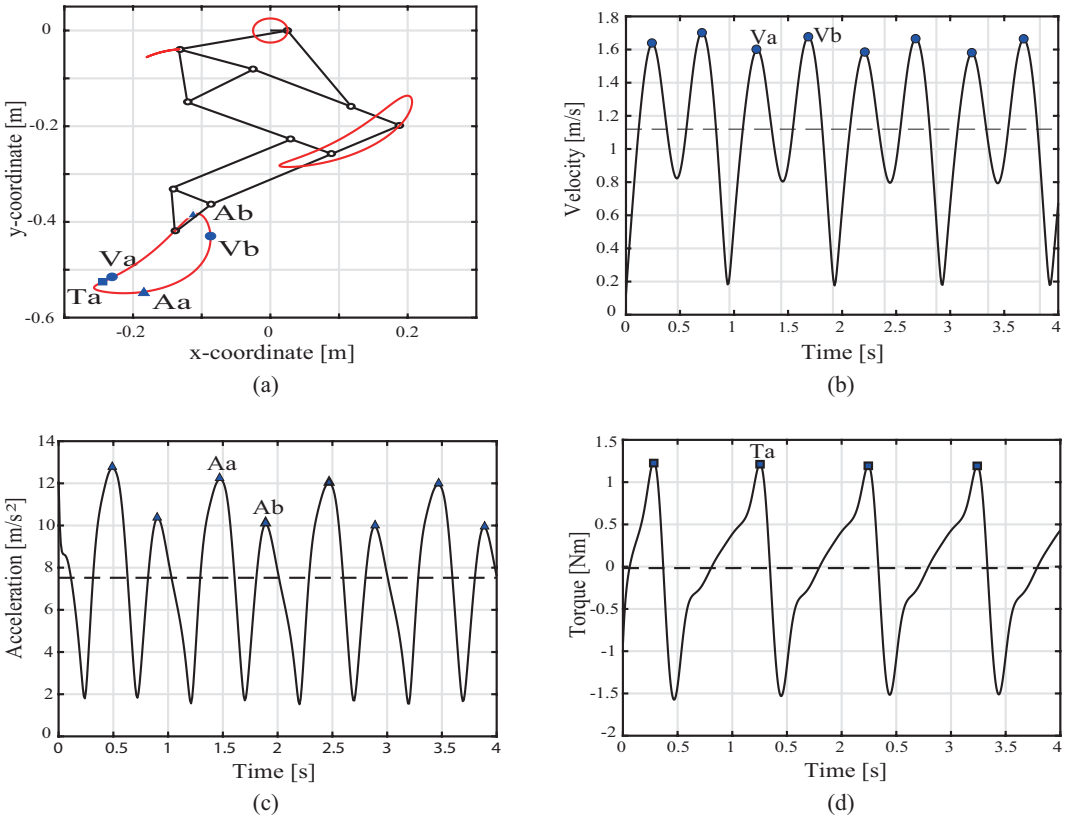

Figure 6-6: Comparison of the common factors in relation to length of L_3 link

The distance driver inserted to the linkage as function of muscle tendon unit and its constraint formulation was considered. The results presents detailed information on the effect of changes of linear displacement in distance driver measured on velocity, acceleration and power consumption of driving link as shown in Figure 6-6. The result shows that biologically inspired closed linkage mechanism driven by cyclic motion can be energy efficient and adaptable with the sudden change of the environment were presented by different modifiable leg trajectory. The validity of the horse leg mechanism was confirmed successfully in terms of both range of motion and kinematics. The important finding is that a kicking force is generated in the toe just before the grounding as shown clearly in acceleration plot in Figure 6-5(c). The non-linear kinematic transmission in length change of link may provide a hint to analyze adaptive capabilities in the animal locomotion even by the simple closed linkage without a complex actuator control system. Furthermore, in applying appro-

priate driver constraint in system as principle movement strategy in running animal functional and animal-like end trajectories were generated and evaluated with duty factor which defines the specific locomotor behaviour with respect to the stance and swing timing in one locomotive cycle by Batbaatar & Wagatsuma (2020) [89].

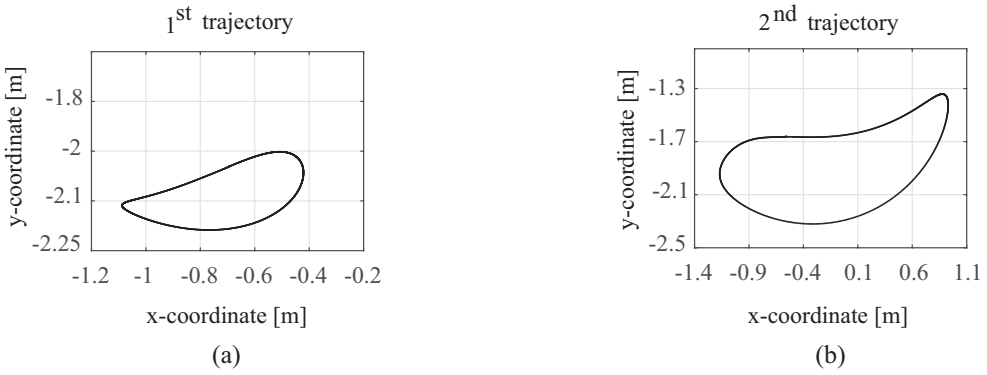

Figure 6-7: Gait trajectories generated from the horse leg motion. Walking (a), Running (b).

Two trajectories were selected as typical trajectories to reproduce walking and running gaits according to the mechanics of the simple model, which are generated by changing the control parameters associated with driver constraint in the horse leg mechanism. As shown in Figure 2, the 1^{st} trajectory considered to be a walking in term of duty factor and step length, the relation was evaluated in previous study. The 2^{nd} trajectory which has longer step length compared to the 1^{st} trajectory considered to be running gait in which leg orientation controlled by swinging motion with respect to the body, which may potentially generate the propulsive ground reaction force due the intrinsic high rate of angular oscillation at the hoof. In addition, the motion analysis can be developed following two points. The first point is a consideration of replacement of elastic links in a part. According to the theory of the flexible multibody dynamics [47], our analysis seamlessly can be extended to the flexible multibody dynamics, which may improve the efficacy to absorb the ground reaction force when grounding of the leg. The second point is the ground reaction analysis to require an introduction of the extra component as the ground surface can be formulated according the the contact force model in Chapter 3 of this thesis. The third point

is the visualization of the ground reaction force because there are different type of contact occurs in hoof of leg mechanism with ground in comparison with pointed contact by Chebyshev and Theo-Jansen mechanism. It is reflected to the condition with determination of multiple points in contact as illustrated:

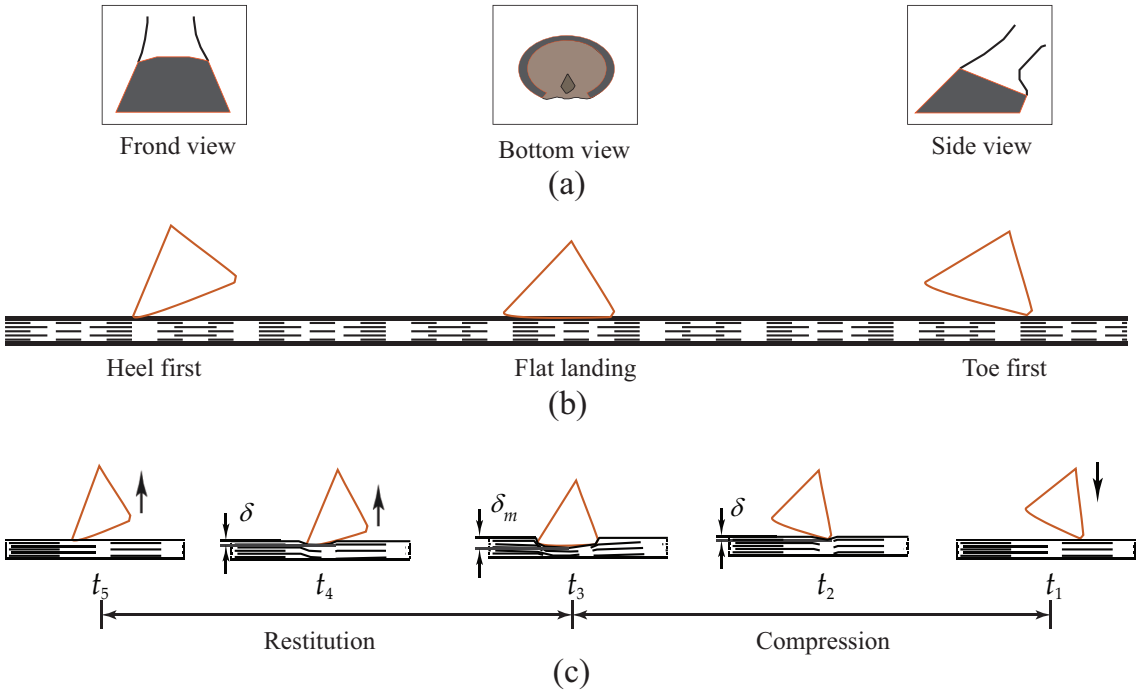

Figure 6-8: Different viewpoint of hoof wall (a), Possible contact types depending on landing of the hoof on ground (b), Representation of impact between hoof and ground for the case of toe first landing (c)

As shown in Figure 6-8(c), there are three types of possible foot-ground contact occurs, namely, heel first, toe first, flat, or multiple point contact. In consideration of rolling hoof motion in contact with the ground: firstly, contact force should be treated systematically to assemble sequence of impulses in order to determine the exact shape of ground reaction force considering the complete gait cycle of leg motion. Secondly, hoof-ground interaction imposes large local elastic deformation where a biological animal absorbs the energy in passive elastic tendons that are used in the energy interconversion during the locomotion cycle explained in articles [90, 91].

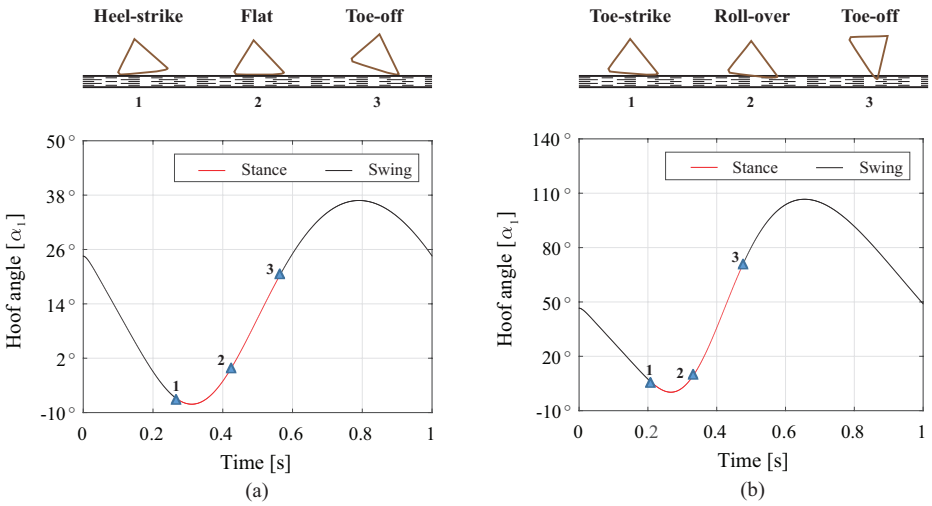

Figure 6-9: Hoof angle variations with respect to the locomotive trajectory. Angular rotation of hoof in one locomotive cycle of walking gait (a) and running gait (b).

In the temporal evaluation of the hoof angle as shown in Figure 6-9, walking and running gaits were generated in accordance with the first and second trajectories in Figure 6-7. In the waling gait, the transition of sub-phases commonly occurred in the rolling motion of the triangle structure in both cases. In the walking gait, those sub-phases from heel-strike, flat and toe-off were gradually generated (Figure 6-9 top-left), which is consistent with the gradual change of the hoof angle (Figure 6-9 bottom-left), while in the running gait, the transition started from the toe-strike that causes the roll-over sub-phase quickly and then reached to the toe-off sub-phase with a large gap from the ground rather than that in the walking gait. The result was numerically examined as the first contact occurs at instant time $t_1 = 0.267s$ and $\alpha_1 = -6.83°$ leaves the ground at $t_3 = 0.569s$ and $\alpha_1 = -20.9°$ for the 1^{st} (walking) trajectory. In the case, the hoof rolling over the ground and during the mid-stance multiple contact points were examined at $\alpha_1 = -0.23°$ degree in which hoof was almost parallel with the ground. When the hoof leaves the ground, angular variation during the contact phase was reached 26° degrees. For the 2^{nd} (running) trajectory, the contact phenomenon occurred at the instant time $t_1 = 0.208s$ and $\alpha_1 = 6.20°$ firstly, shifted to leaving from the ground at $t_3 = 0.478s$ and $\alpha_1 = 71.08°$. Finally, the hoof angle was reached 64.8° degrees, which is approximately 2.5 times larger than the result in the walking gait. Interestingly, the hoof-ground interaction

was significantly influenced by the initial impact phenomenon, which differentiate the grounding part either heel or toe and it reflects to successive sub-phases too. Even in the simple model, the differentiation was clearly observed not only in the trajectory level as a posture and kinematic analysis but also in the kinetic level as the dynamics analysis, which is easily extended to the energy analysis. All these sub-phases are characterized as representative sub-phase to reconstruct the target gait and it can provide the parametric analysis with stiffness and damping, which is associated with an actual parameter from soft tissues in the distal limb. It is because that the compliant contact force model was theoretically described as shown in the method section, which allow to change those parameters related to reaction forces easily.

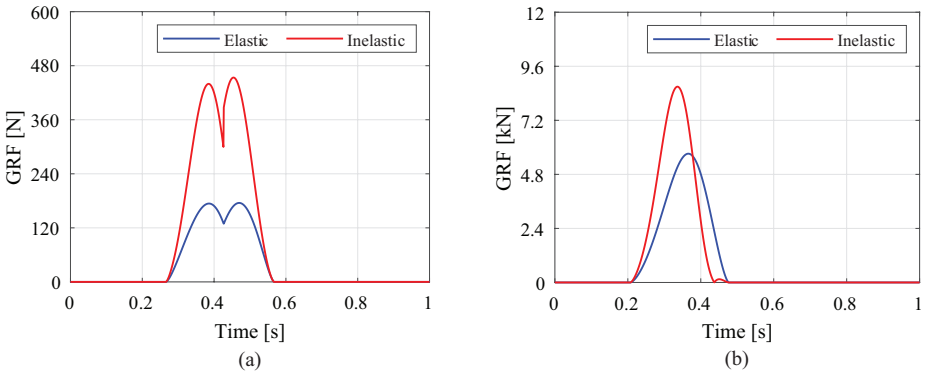

Figure 6-10: Resultant values of ground reaction forces under the different contact condition. Force pattern of walking gait (a) and running gait (b).

In the MATLAB based numerical simulation, ground reaction forces were evaluated by using Lankarani & Nikravesh [45] model by changing restitution coefficients as $cr = 1.0$ for elastic and $cr = 0$ for inelastic contact cases. According to the analysis, the maximum contact force was obtained as 453.65N for the 1^{st} (walking) trajectory in the inelastic contact condition and 175.34N in the elastic case. Average normal force was 80.83N and 34.88N respectively. For the 2^{nd} (running) trajectory, the maximum GRF was 8.694kN for the inelastic contact condition and 5.719kN in the elastic case. Average normal force was 978N and 800N respectively. Result showed that the significant reduction of ground reaction force with respect to the viscoelastic con-

tact was estimated as 61.35% in 1^{st} trajectory and 34.22% in 2^{nd} trajectory. In the walking trajectory, multiple point support occurring in which hoof loaded the body weight at mid-stance as shown in Figure 6-10 (a), the maximum pressure or force peak indicated in only when the leg first impact and leaves the ground which was consistent with the force pattern observed in the human walking gait [92, 90].

Chapter 7

Discussion and Conclusion

In the previous study by Komoda & Wagatsuma [7], which investigated a similar comparison of the energy consumption of different closed-loop mechanisms, their results were not considered about the interaction of the leg and the ground surface. The ground reaction is highly important as shown by Corral et al. [46], which investigated best ranges of coefficients for restitution and friction to realize a sustainable walking motion. As Nikooyan & Zadpoor [11] discussed in their theoretical study, a significant contribution of the ground reaction force appears in muscle fatigue due to human running because a soft tissue vibration in the physiological body is triggered by the impact force when the leg is grounding, which can be modeled by a mass-spring-damper model. According to the model by Clark et al. [12], the ground contact mechanism in human running has two steps and then the total ground reaction force is composed of the collision of the lower limb and the concurrent vertical accelerations of the rest of the body during ground contact. Phenomenologically, in their study, the ground reaction force is observed as a bell-shape impact at the first moment in the stance phase, known as a rocking chair mechanism, and interestingly in the present study a bell-shaped peak in the early stance phase was similarly observed in the torque in the inverse dynamics in the case of the Theo-Jansen mechanism as shown in Figure 4-10. The human leg mechanism is more complex rather than walking linkages, while our computer experiment showed a possibility to analyze the spring-damper effect owing to a flexibility of the ankle region as a common

tendency of the walking and running mechanism in a simple manner. However, the second component due to leaning of the entire body weight into the leg is not explained by walking linkages if they are stable vertically without releasing the fixation of the rotation center as discussed by Komoda & Wagatsuma (2015) [49] or further development of the linkage to mimic an realistic animal leg motion by Batbaatar & Wagatsuma [5]. In the mechanical and material mechanics points of view, the elastic deformation has the benefit to store and release energy in the locomotion cycle [90, 91], which may inspire an energy regeneration in the actuator design [93, 94]. If an appropriate energy regeneration [95] and automatic compliance control [25] is possible based on the linkage system with elastic materials without electromechanical complex systems, it has a large impact to the robotic system design to reduce the size and cost. The proposed scheme contributes to the detail analysis in those purposes. In regard to the nonlinear property of dissipative contact force models, we introduced the model by Lankarani & Nikravesh [45] as the traditional one, while the detail comparison is possible to analyze by replacing other nonlinear models such as Flores et al.[55] and Hu & Guo [30]. In the present study, the dissipative contact force model is integrated computationally to focus on the energy consumption of different walking linkages for minimizing numerical errors due to the complexity of the formulation, which is consistent with the approach of Flores and Ambrósio [67], while if an interaction with the ground surface with geometric changes is crucial, there exists a further extension of the differential-algebraic system as Equation (2.8) including the vector of non-generalized surface parameters under the consideration of geometric parameters separately from absolute coordinates formulated by Rathod & Shabana [96]. For the sake of analyses of closed-linkage walking mechanisms in the viewpoint, we proposed the computational scheme to integrate formulations of the multibody dynamics and a dissipative contact force model in a replaceable way to enable a precise numerical evaluation including inverse dynamics, which was crucial for the evaluation of the energy consumption of different walking mechanisms. In the present study, the effect of viscoelastic ground contact was successfully proved to reduce the energy consumption commonly in Chebyshev and Theo-Jansen walking

mechanisms by using our integrative method of the multibody dynamics with the dissipative contact force model. In the binary condition of the coefficient of restitution in the damping factor model by Lankarani & Nikravesh [45], the perfectly elastic impact reduced 31.4% and 61.2% energy consumption with respect to the inelastic impact respectively in cases of Chebyshev and Theo-Jansen mechanisms in the same clockwise rotation of the input driver. In the consideration of the moving direction, the counter-clockwise rotation of the input driver is necessary in the Theo-Jansen mechanism, and if it has no elasticity in the ground contact the bell-shaped torque requirement was arisen for a constant rotation of the input driver, which was not observed in the Chebyshev mechanism. The phenomenon reflects to an impact force against the ground and it implies the generation of a locomotive power for going forward, or kicking the ground. The viscoelasticity effectively absorbs the impact in the stance phase and significantly contributes to the reduction of the energy consumption.

Bibliography

[1] Sack W. O. Rock S. Horowitz A. Berg R. Budras, K. D. *Pelvic Limb*. Schlueter-sche, 2012.

[2] Daniel Giesbrecht, Christine Q. Wu, and Nariman Sepehri. Design and optimization of an eight-bar legged walking mechanism imitating a kinetic sculpture, "Wind Beast". *Transactions of the Canadian Society for Mechanical Engineering*, 36:343–355, 2012.

[3] Shivamanappa G. Desai, Anandkumar R. Annigeri, and A. TimmanaGouda. Analysis of a new single degree-of-freedom eight link leg mechanism for walking machine. *Mechanism and Machine Theory*, 140:747–764, 2019.

[4] Shunsuke Nansai, Rajesh Elara Mohan, Ning Tan, Nicolas Rojas, and Masami Iwase. Dynamic modeling and nonlinear position control of a quadruped robot with theo jansen linkage mechanisms and a single actuator. *Journal of Robotics*, 2015, 2015.

[5] Dondogjamts Batbaatar and Hiroaki Wagatsuma. A proposal of the kinematic model of the horse leg musculoskeletal system by using closed linkages. In *IEEE International Conference on Robotics and Biomimetics*, pages 869–874, 2019.

[6] Lalit Patnaik and Loganathan Umanand. Kinematics and dynamics of Jansen leg mechanism: A bond graph approach. *Simulation Modelling Practice and Theory*, 60:160–169, 2016.

[7] Kazuma Komoda and Hiroaki Wagatsuma. Energy-efficacy comparisons and multibody dynamics analyses of legged robots with different closed-loop mechanisms. *Multibody System Dynamics*, 40:123–153, 2017.

[8] P. E. Nikravesh. *Planar Multibody Dynamics: Formulation, Programming and Applications*. CRC Press, 2007.

[9] Parviz E Nikravesh. *Planar multibody dynamics: formulation, programming with Matlab, and applications*. CRC Press, second edition, 2019.

[10] Arkady S. Voloshin, Joseph Mizrahi, Oleg Verbitsky, and Eli Isakov. Dynamic loading on the human musculoskeletal system effect of fatigue. *Clinical Biomechanics*, 13:515–520, 1998.

[11] Ali Asadi Nikooyan and Amir Abbas Zadpoor. Effects of muscle fatigue on the ground reaction force and soft-tissue vibrations during running: A model study. *IEEE Transactions on Biomedical Engineering*, 59:797–804, 2012.

[12] Kenneth P. Clark, Laurence J. Ryan, and Peter G. Weyand. A general relationship links gait mechanics and running ground reaction forces. *Journal of Experimental Biology*, 220:247–258, 2017.

[13] Sebastian Skals, Moon Ki Jung, Michael Damsgaard, and Michael S. Andersen. Prediction of ground reaction forces and moments during sports-related movements. *Multibody System Dynamics*, 39:175–195, 2017.

[14] Yoshiaki Sakagami, Ryujin Watanabe, Chiaki Aoyama, Shinichi Matsunaga, Nobuo Higaki, and Kikuo Fujimura. The intelligent ASIMO: System overview and integration. *IEEE International Conference on Intelligent Robots and Systems*, 3:2478–2483, 2002.

[15] Guangrong Chen, Junzheng Wang, and Lipeng Wang. Gait planning and compliance control of a biped robot on stairs with desired ZMP. *IFAC Proceedings Volumes*, 19:2165–2170, 2014.

[16] D Astudillo, L I Minchala, F Astudillo-Salinas, A Vazquez-Rodas, and L Gonzalez. A simple mapping methodology of gait biomechanics for walking control of a biped robot. In *2018 IEEE XXV International Conference on Electronics, Electrical Engineering and Computing (INTERCON)*, pages 1–4, Aug 2018.

[17] Guangrong Chen, Junzheng Wang, Shoukun Wang, Jiangbo Zhao, and Wei Shen. Energy saving control in separate meter in and separate meter out control system. *Control Engineering Practice*, 72:138–150, 2018.

[18] Chan Lee, Suhui Kwak, Jihoo Kwak, and Sehoon Oh. Generalization of Series Elastic Actuator configurations and dynamic behavior comparison. *Actuators*, 6, 2017.

[19] Felix Ruppert and Alexander Badri-Spröwitz. Series elastic behavior of biarticular muscle-tendon structure in a robotic leg. *Frontiers in Neurorobotics*, 13:1–13, 2019.

[20] E. Garcia, J. C. Arevalo, G. Muoz, and P. Gonzalez-De-Santos. Combining series elastic actuation and magneto-rheological damping for the control of agile locomotion. *Robotics and Autonomous Systems*, 59:827–839, 2011.

[21] Xiaomin Dong, Weiqi Liu, Xuhong Wang, Jianqiang Yu, and Pinggen Chen. Research on variable stiffness and damping magnetorheological actuator for robot joint. *Lecture Notes in Computer Science (including subseries Lecture Notes in Artificial Intelligence and Lecture Notes in Bioinformatics)*, 10464 LNAI:109–119, 2017.

[22] Marc H. Raibert. Running with symmetry. *The International Journal of Robotics Research*, 5(4):3–19, 1986.

[23] Alan M. Wilson, M. Polly McGuigan, Anne Su, and Anton J. Van den Bogert. Horses damp the spring in their step. *Nature*, 414(6866):895–899, 2001.

[24] Z. H. Shen and J. E. Seipel. A fundamental mechanism of legged locomotion with hip torque and leg damping. *Bioinspiration and Biomimetics*, 7, 2012.

[25] Jie Chen, Zhongchao Liang, Yanhe Zhu, Chong Liu, Lei Zhang, Lina Hao, and Jie Zhao. Towards the exploitation of physical compliance in segmented and electrically actuated robotic legs: A review focused on elastic mechanisms. *Sensors (Switzerland)*, 19, 2019.

[26] An Mo, Fabio Izzi, Daniel F.B. Haeufle, and Alexander Badri-Spröwitz. Effective Viscous Damping Enables Morphological Computation in Legged Locomotion. *Frontiers in Robotics and AI*, 7:1–22, 2020.

[27] Steve Heim, Matthew Millard, Charlotte Le Mouel, and Alexander Badri-Spröwitz. A little damping goes a long way: A simulation study of how damping influences task-level stability in running: A little damping goes a long way. *Biology Letters*, 16, 2020.

[28] Daniel F. B. Haeufle, Katrin Stollenmaier, Isabelle Heinrich, Syn Schmitt, and Keyan Ghazi-Zahedi. Morphological Computation Increases From Lower- to Higher-Level of Biological Motor Control Hierarchy. *Frontiers in Robotics and AI*, 7:1–13, 2020.

[29] Ozgur Baser, Hasbi Kizilhan, and Ergin Kilic. Employing variable impedance (stiffness/damping) hybrid actuators on lower limb exoskeleton robots for stable and safe walking trajectory tracking. *Journal of Mechanical Science and Technology*, 34:2597–2607, 2020.

[30] S. Schmitt, D. F.B. Haeufle, R. Blickhan, and M. Günther. Nature as an engineer: One simple concept of a bio-inspired functional artificial muscle. *Bioinspiration and Biomimetics*, 7, 2012.

[31] Jong Shi Pang and Jeffrey C. Trinkle. Complementarity formulations and existence of solutions of dynamic multi-rigid-body contact problems with Coulomb friction. *Mathematical Programming, Series B*, 73:199–226, 1996.

[32] P. Song, P. Kraus, V. Kumar, and P. Dupont. Analysis of rigid-body dynamic models for simulation of systems with frictional contacts. *Journal of Applied Mechanics, Transactions ASME*, 68:118–128, 2001.

[33] Pierre E. Dupont and Serge P. Yamajako. Stability of frictional contact in constrained rigid-body dynamics. *IEEE Transactions on Robotics and Automation*, 13:230–236, 1997.

[34] Mihai Anitescu, Andrew Miller, and Gary D. Hart. Constraint stabilization for time-stepping approaches for rigid multibody dynamics with joints, contact, and friction. *Proceedings of the ASME Design Engineering Technical Conference*, 5 B:1071–1080, 2003.

[35] Georg-P. Ostermeyer. On Baumgarte Stabilization for Differential Algebraic Equations. In Edward J Haug and Roderic C Deyo, editors, *Real-Time Integration Methods for Mechanical System Simulation*, pages 193–207. Springer Berlin Heidelberg, 1990.

[36] J. Baumgarte. Stabilization of constraints and integrals of motion in dynamical systems. *Computer Methods in Applied Mechanics and Engineering*, 1:1–16, 1972.

[37] P. Flores. A study on constraints violation in dynamic analysis of spatial mechanisms. *Mechanisms and Machine Science*, 50:593–601, 2018.

[38] Javier García de Jalón. *Kinematic and Dynamic Simulation of Multibody Systems The Real-Time Challenge*, volume 71. 1994.

[39] Denis S. Goldobin, Eugeniy A. Susloparov, Anastasiya V. Pimenova, and Nikolai V. Brilliantov. Collision of viscoelastic bodies: Rigorous derivation of dissipative force. *European Physical Journal E*, 38, 2015.

[40] Paulo Flores and Hamid M Lankarani. *Contact Force Models for Multibody Dynamics*, volume 226. Springer, 2016.

[41] Werner Goldsmith and J. T. Frasier. *Impact: The Theory and Physical Behavior of Colliding Solids*, volume 28. E. Arnold, 1961.

[42] K. H. Hunt and F. R.E. Crossley. Coefficient of Restitution Interpreted As Damping in Vibroimpact. *American Society of Mechanical Engineers (Paper)*, 42:440–445, 1975.

[43] Dahai Zhao and Yong Liu. Improved Damping Constant of Hertz-Damp Model for Pounding between Structures. *Mathematical Problems in Engineering*, 2016, 2016.

[44] Shiwu Hu and Xinglin Guo. A dissipative contact force model for impact analysis in multibody dynamics. *Multibody System Dynamics*, 35:131–151, 2015.

[45] H. M. Lankarani and P. E. Nikravesh. A contact force model with hysteresis damping for impact analysis of multibody systems. *Journal of Mechanical Design, Transactions of the ASME*, 112:369–376, 1990.

[46] Eduardo Corral, M. J.Gómez García, Cristina Castejon, Jesús Meneses, and Raúl Gismeros. Dynamic modeling of the dissipative contact and friction forces of a passive biped-walking robot. *Applied Sciences (Switzerland)*, 10, 2020.

[47] Ahmed A. Shabana. *Constrained Dynamics*. John Wiley & Sons, Ltd, third edition, 2009.

[48] Stephen Levin, Susan Lowell de Solórzano, and Graham Scarr. The significance of closed kinematic chains to biological movement and dynamic stability. *Journal of Bodywork and Movement Therapies*, 21:664–672, 2017.

[49] Kazuma Komoda and Hiroaki Wagatsuma. A Determinant Analysis to Detect the Singularity of the Extended Theo Jansen Mechanism in the Phase-Rotation-Amplitude Parameter Space. *Journal of Computer Science & Systems Biology*, 09:10–22, 2015.

[50] R. A. Wehage and E. J. Haug. Generalized coordinate partitioning for dimension reduction in analysis of constrained dynamic systems. *Journal of Mechanical Design, Transactions of the ASME*, 104:247–255, 1982.

[51] Paulo Flores, Margarida MacHado, Eurico Seabra, and Miguel Tavares Da Silva. A parametric study on the baumgarte stabilization method for forward dynamics of constrained multibody systems. *Journal of Computational and Nonlinear Dynamics*, 6(1), 2011.

[52] Pedro Moreira, Miguel Silva, and Paulo Flores. Ground foot interaction in human gait: modelling and simulation. *7th EUROMECH Solid Mechanics Conference. Lisbon, ...*, (June 2014):1–13, 2009.

[53] Valentin L. Popov. *Contact between Rough Surfaces*. Springer Berlin Heidelberg, 2010.

[54] Heinrich Hertz. Ueber die Berührung fester elastischer Körper. *Journal fur die Reine und Angewandte Mathematik*, 1882:156–171, 1882.

[55] Paulo Flores, Margarida MacHado, Miguel T. Silva, and Jorge M. Martins. On the continuous contact force models for soft materials in multibody dynamics. *Multibody System Dynamics*, 25:357–375, 2011.

[56] Luka Skrinjar, Janko Slavič, and Miha Boltežar. A review of continuous contact-force models in multibody dynamics. *International Journal of Mechanical Sciences*, 145:171–187, 2018.

[57] Jie Zhang, Wenhao Li, Lei Zhao, and Guangping He. A continuous contact force model for impact analysis in multibody dynamics. *Mechanism and Machine Theory*, 153:103946, 2020.

[58] Najmeh Ghorbani and Ahmadreza Pishevar. A mesoscopic simulation of static and dynamic wetting using many-body dissipative particle dynamics. *Computational Particle Mechanics*, 5:113–123, 2018.

[59] J A C Ambrósio. *Impact of Rigid and Flexible Multibody Systems: Deformation Description and Contact Models*, pages 57–81. Springer Netherlands, Dordrecht, 2003.

[60] V. P. Chervinskii. Dissipative function of coulomb friction on elliptical contact area. *Journal of Friction and Wear*, 32:386–393, 2011.

[61] Filipe Marques, Paulo Flores, J. C.Pimenta Claro, and Hamid M. Lankarani. Modeling and analysis of friction including rolling effects in multibody dynamics: a review. *Multibody System Dynamics*, 45:223–244, 2019.

[62] Ahmed A. Shabana, Khaled E. Zaazaa, and Hiroyuki Sugiyama. *Railroad Vehicle Dynamics: A Computational Approach*. CRC Press, Inc., USA, 1st edition, 2007.

[63] Gerald Ristow. Simulating granular flow with molecular dynamics. *Journal de Physique I, EDP Sciences*, 2:649–662, 1992.

[64] Galina Kuteeva, Boris Ershov, and Tatiana Voloshinova. Models of mechanisms by P. L. Chebyshev in St. Petersburg University. *2015 International Conference on Mechanics - Seventh Polyakhov's Reading*, pages 1–3, 2015.

[65] T. Jansen. *The Great Pretender*. Netherlands:010, 2007.

[66] Joseph Edward Shigley. The mechanics of walking vehicles: a feasibility study: final report. Technical report, University of Michigan Research Institute, 1960.

[67] Paulo Flores and Jorge Ambrósio. On the contact detection for contact-impact analysis in multibody systems. *Multibody System Dynamics*, 24:103–122, 2010.

[68] Kenneth J. Waldron and Gary L. Kinzel. Relationship Between Actuator Geometry and Mechanical Efficiency in Robots. pages 366–374, 1981.

[69] M. Anitescu and F. A. Potra. Formulating Dynamic Multi-Rigid-Body Contact Problems with Friction as Solvable Linear Complementarity Problems. *Nonlinear Dynamics*, 14:231–247, 1997.

[70] Burak Demirel, M. Tolga Emirler, Ümit Sönmez, and Ahmet Yörükoğlu. Semi-compliant force generator mechanism design for a required impact and contact forces. *Journal of Mechanisms and Robotics*, 2:1–11, 2010.

[71] M. J.D. Powell. Algorithms for nonlinear constraints that use lagrangian functions. *Mathematical Programming*, 14:224–248, 1978.

[72] Li Xin Xu. A method for modelling contact between circular and non-circular shapes with variable radii of curvature and its application in planar mechanical systems. *Multibody System Dynamics*, 39:153–174, 2017.

[73] T. McGeer. Passive Dynamic Walking. *The International Journal of Robotics Research*, 9:62–82, 1990.

[74] Buehler M. Campbell, D. Preliminary bounding experiments in a dynamic hexapod. *Experimental Robotics*, 8:612–621, 2003.

[75] Ahmadi M. Buehler M. Gregorio, P. esign, control, and energetics of an electrically actuated legged robot. *IEEE Trans. Syst. Man Cybern., Part B, Cybern.*, 27:626–634, 1997.

[76] Chen C. Li W. Jin, B. Power consumption optimization for a hexapod walking robot. *J. Intell. Robot. Syst.*, 71:195–209, 2013.

[77] M. Hildebrand. Symmetrical Gaits of Horses. *Science*, 150:701–708, 1965.

[78] Taylor C. R. Hoyt, D. F. Gait and the energetic of locomotion in horses. *Nature*, 292:239–240, 1981.

[79] Robilliard J. J. Weller R. Wilson A. M. Pfau T. Starke, S. D. Walk–run classification of symmetrical gaits in the horse: a multidimensional approach. *J R Soc Interface.*, 6:335–342, 2009.

[80] Huang Y.-J. Lin W.-C. Huang, T.-C. Real-time Horse Gait Synthesis. *Comp. Anim. Virtual Worlds 2013*, 24:87–95, 2012.

[81] Moeslund T. B. Fihl, P. Invariant gait continuum based on the duty-factor. *Signal, Image and Video Processing*, 3:391–402, 2009.

[82] Wagatsuma H. Komoda, K. Singular configurations analyses of the modifiable Theo Jansen-like mechanism by focusing on the Jacobian determinant—a finding limitations to exceed normal joint range of motion. In *Proceedings of 2014 IEEE/ASME International Conference on Advanced Intelligent Mechatronics (AIM)*, volume 75, pages 76–81, 2014.

[83] M. Rajesh Elara R. Sosa S. Nansai, N. Rojas and M. Iwase. On a Jansen Leg with Multiple Gait Patterns for Reconfigurable Walking Platforms. *Advances in Mechanical Engineering*, 7:1–18, 2015.

[84] Thomaszewski B. Noris G. Sueda S. Forberg M. Sumner R. W. Matusik W. Bickel B. Coros, S. Computational Design of Mechanical Characters. *ACM Transactions on Graphics (TOG)*, 32, 1987.

[85] Van den Bogert A.J. Hartman A.B.W. Kersjes A.W. Van Weeren, P.R. The role of the reciprocal apparatus in the hind limb of the horse investigated by a modified CODA-3 opto-electronic kinematic analysis system. *Equine Vet. J. Suppl.*, 9:95–100, 1990.

[86] G. J. Molenaar. Kinematics of the Reciprocal Apparatus in the Horse. *Anatomia, Histologia, Embryologia*, 12:278–287, 1983.

[87] M. Hildebrand. The Mechanics of Horse Legs. *American Scientist*, 75:594–601, 1987.

[88] M. Muller. A novel classification of planar four-bar linkages and its application to the mechanical analysis of animal systems. *Philos. Trans. R. Soc. Lond.*, 351:689–720, 1996.

[89] D. Batbaatar and H. Wagatsuma. An extension of kinematic model for the linkage mechanism to analyze the workspace and gait trajectory induced by the

swing leg motion. In *2020 3rd International Conference on Control and Robots (ICCR)*, pages 57–64, 2020.

[90] R. Mcneill Alexander. Elastic energy stores in running vertebrates. *Integrative and Comparative Biology*, 24(1):85–94, 1984.

[91] Andrew A. Biewener. Muscle-tendon stresses and elastic energy storage during locomotion in the horse. *Comparative Biochemistry and Physiology - B Biochemistry and Molecular Biology*, 120:73–87, 1998.

[92] R. Mc Neill Alexander. Energetics and optimization of human walking and running: The 2000 Raymond Pearl Memorial Lecture. *American Journal of Human Biology*, 14(5):641–648, 2002.

[93] Patrick M. Wensing, Albert Wang, Sangok Seok, David Otten, Jeffrey Lang, and Sangbae Kim. Proprioceptive actuator design in the MIT cheetah: Impact mitigation and high-bandwidth physical interaction for dynamic legged robots. *IEEE Transactions on Robotics*, 33:509–522, 2017.

[94] Hae-Won Park and Sangbae Kim. The MIT Cheetah, an Electrically-Powered Quadrupedal Robot for High-speed Running. *Journal of the Robotics Society of Japan*, 32:323–328, 2014.

[95] Sangok Seok, Albert Wang, Meng Yee Chuah, Dong Jin Hyun, Jongwoo Lee, David M. Otten, Jeffrey H. Lang, and Sangbae Kim. Design principles for energy-efficient legged locomotion and implementation on the MIT Cheetah robot. *IEEE/ASME Transactions on Mechatronics*, 20:1117–1129, 2015.

[96] Cheta Rathod and Ahmed A. Shabana. Geometry and differentiability requirements in multibody railroad vehicle dynamic formulations. *Nonlinear Dynamics*, 47:249–261, 2007.

Research achievements

Papers presented in this thesis

Journal paper

1. **D. Batbaatar** and H. Wagatsuma, "A computational framework to be able to evaluate the energy conservation effect in viscoelastic ground contact in cases of closed-loop walking mechanisms," .

2. **D. Batbaatar** and H. Wagatsuma, "A viscoelastic contact analysis of the ground reaction force differentiation in walking and running gaits realized in the simplified horse leg model focusing on the hoof-ground interaction", *Journal of Robotics, Networking and Artificial Life, Atlantis press.*

Peer reviewed papers presented in international conferences

1. **D. Batbaatar** and H. Wagatsuma, "An Extension of Kinematic Model for the Linkage Mechanism to Analyze the Workspace and Gait Trajectory Induced by the Swing Leg Motion," *2020 IEEE International Conference on Control and Robotics (ICCR)*,Tokyo, Japan,2020, pp. 57–64.

2. **D. Batbaatar** and H. Wagatsuma, "A Proposal of the Kinematic Model of the Horse Leg Musculoskeletal System by Using Closed Linkages," *2019 IEEE International Conference on Robotics and Biomimetics (ROBIO)*, pp. 869–874, 2019.